AGU PUBLICATIONS

Tectonics

RESEARCH ARTICLE
10.1002/2015TC003864

Key Points:
- The CAFZ is a weakly active transtensional fault system
- Minimum sinistral slip rate of 1.1 ± 0.3 mm a^{-1}
- Evidence is presented which reveals ESE-WNW extension since 2.73 Ma

Supporting Information:
- Text S1 and Tables S1–S10

Correspondence to:
M. Higgins,
mark.higgins@mail.utoronto.ca

Citation:
Higgins, M., L. M. Schoenbohm, G. Brocard, N. Kaymakci, J. C. Gosse, and M. A. Cosca (2015), New kinematic and geochronologic evidence for the Quaternary evolution of the Central Anatolian fault zone (CAFZ), *Tectonics*, *34*, doi:10.1002/2015TC003864.

Received 10 MAR 2015
Accepted 2 SEP 2015
Accepted article online 5 SEP 2015

New kinematic and geochronologic evidence for the Quaternary evolution of the Central Anatolian fault zone (CAFZ)

Mark Higgins[1], Lindsay M. Schoenbohm[1], Gilles Brocard[2], Nuretdin Kaymakci[3], John C. Gosse[4], and Michael A. Cosca[5]

[1]Department of Earth Sciences, University of Toronto, Toronto, Ontario, Canada, [2]Department of Earth and Environmental Science, University of Pennsylvania, Philadelphia, Pennsylvania, USA, [3]Department of Geological Engineering, Middle East Technical University, Ankara, Turkey, [4]Department of Earth Sciences, Dalhousie University, Halifax, Nova Scotia, Canada, [5]Central Mineral and Environmental Resources Science Center, U.S. Geological Survey, Denver, Colorado, USA

Abstract As the kinematics of active faults that bound the Anatolian plate are well studied, it is now essential to improve our understanding of the style and rates of intraplate deformation to constrain regional strain partitioning and improve seismic risk assessments. One of these internal structures, the Central Anatolian fault zone (CAFZ), was originally defined as a regionally significant left-lateral "tectonic escape" structure, stretching for 700 km in a NE direction across the Anatolian plate. We provide new structural, geomorphic, and geochronologic data for several key segments within the central part of the CAFZ that suggest that the sinistral motion has been overstated. The Ecemiş fault, the southernmost part of the CAFZ, has a late-Quaternary minimum slip rate of 1.1 ± 0.4 mm a^{-1}, slower than originally proposed. Farther north, the Erciyes fault has fed a linear array of monogenetic vents of the Erciyes stratovolcano and $^{40}Ar/^{39}Ar$ dating shows a syneruptive stress field of ESE-WNW extension from 580 ± 130 ka to 210 ± 180 ka. In the Erciyes basin, and central part of the CAFZ, we mapped and recharacterized the Erkilet and Gesi faults as predominantly extensional. These long-term geological rates support recent GPS observations that reveal ESE-WNW extension, which we propose as the driver of faulting since 2.73 ± 0.08 Ma. The slip rates and kinematics derived in this study are not typical of an "escape tectonic" structure. The CAFZ is a transtensional fault system that reactivates paleotectonic structures and accommodates E-W extension associated with the westward movement of Anatolia.

1. Introduction

Lateral escape of microplates is a common feature of active collisional tectonics and has been described in various regions including Tibet [*Tapponnier et al.*, 1982], Anatolia [*McKenzie*, 1972; *Şengör*, 1985; *Dewey et al.*, 1986], Alaska [*Redfield et al.*, 2007], and Taiwan [*Lacombe et al.*, 2001]. In each case, microplates move away from a zone of collision toward a free boundary or an extending domain [*Burke and Sengör*, 1986]. A debate exists about the driving forces behind the lateral escape of the Anatolian plate, where Arabian plate collision in the Eastern Anatolian combined with ongoing extension in the Western Anatolia associated with retreat of the Hellenic trench (Figure 1) result in rapid westward extrusion. Recent research on the Anatolian plate has focused primarily on its bounding faults, the North and East Anatolian faults, while the style and magnitude of internal deformation have received less attention. Improved understanding of intraplate strain is required to test competing hypotheses.

Conceptual models of the geodynamics of the eastern Mediterranean are complex and varied. *Şengör* [1985] invoked "tectonic escape" in which the westward movement of the Anatolian plate is accommodated by major strike-slip faults, the North Anatolian fault and East Anatolian fault, with relatively insignificant internal deformation. Early GPS studies suggested that present-day motion of the Anatolian plate is explained by coherent extrusion of a rigid tectonic block, driven by the pull of the African slab rollback beneath the Hellenic-Cyprus subduction zones with minimal internal deformation of the plate [*McClusky et al.*, 2000; *Reilinger et al.*, 2006]. Other models call for significant internal deformation of the Anatolian plate, in which smaller strike-slip-bounded crustal wedges move independently, each accommodating some of the relative motion between the Arabian and Eurasian plates [*Şengör*, 1985; *Koçyiğit and Beyhan*, 1998; *Koçyiğit and Erol*, 2001; *Jaffey and Robertson*, 2001; *Bozkurt*, 2001]. The Anatolian plate experienced significant internal deformation

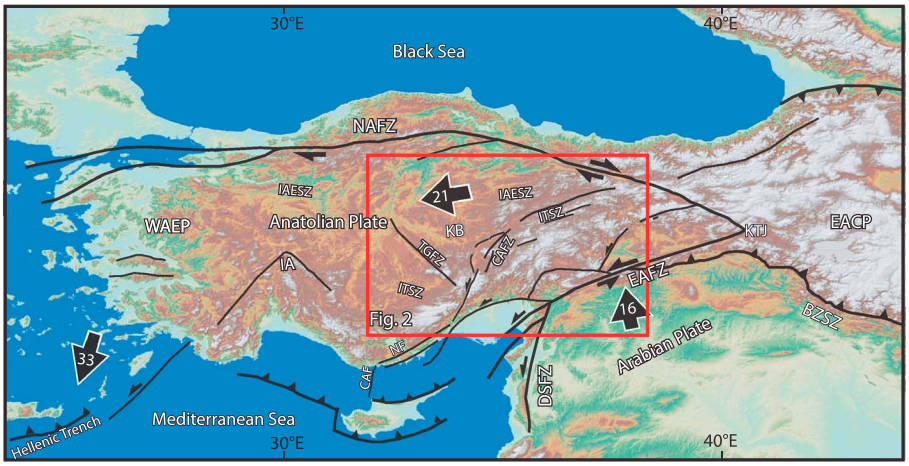

Figure 1. Simplified tectonic map of the eastern Mediterranean showing major plate boundaries and tectonic structures. WEAP: Western Anatolian extensional province, EACP: Eastern Anatolian contractional province [*Şengör*, 1985]. Major plate boundaries in thick black lines, NAFZ: North Anatolian fault zone, EAFZ: East Anatolian fault zone, DSFZ: Dead Sea fault zone. The thin black lines represent second-order tectonic structures of the Anatolian plate, CAFZ: Central Anatolian fault zone, TGFZ: Tüz Gölü fault zone, MOFZ: Malatya-Ovacık fault zone, IA: Isparta angle. Tethyan suture zones in white, IAEZ: Izmir Ankara Erzican suture zone, ITSZ: Inner Tauride suture zone, BZSZ: Bitlis Zagros suture zone, KTJ: Karliova triple junction. The black arrows indicate plate velocities (in mm a^{-1}) from *Reilinger et al.* [2006].

throughout the late Cenozoic, prior to and after the initiation of "escape tectonics," but its contribution to the lateral translation is rarely considered in regional geodynamic models.

In this study, we focus on what is potentially the most significant of these second-order, internal structures, the Central Anatolian fault zone (CAFZ; Figure 1). Previous studies [*Koçyiğit and Beyhan*, 1998; *Toprak*, 1998; *Koçyiğit and Erol*, 2001] classify the CAFZ as a major intracontinental shear zone accommodating compressive strain from the Eastern Anatolian compressional province and have argued for up to 24 km of Pliocene-Quaternary left-lateral displacement [*Koçyiğit and Beyhan*, 1998]. However, its proposed history, connectivity, activity levels, and total left-lateral displacement have been disputed [*Westaway*, 1999; *Westaway et al.*, 2002]. Improved understanding of its activity, kinematics, and tectonic significance is therefore clearly needed. Here we use field mapping, volcanic vent analysis, and terrestrial cosmogenic nuclide and $^{40}Ar/^{39}Ar$ dating to estimate slip rates and characterize the kinematics of several key segments of the southern and central CAFZ. We also compile existing geodetic data and seismic catalogues to help assess the activity of different parts of the fault zone. We propose a model for the Quaternary kinematics and evolution of the CAFZ that requires extrusion-related E-W extension.

2. Background

2.1. Tectonic Setting

The Anatolian plate formed by amalgamation of terranes between Arabia-Africa and Eurasia in the Late Mesozoic. Northward subduction of the African and Arabian plates and closure of distinct Neotethyan seaways are recorded by several prominent suture zones [*Şengör and Yılmaz*, 1981; *Dewey et al.*, 1986], including the Izmir-Ankara-Erzican suture zone (Figure 1) and the Inner Tauride suture zone (Figure 1). The Inner Tauride suture zone separates the Kırşehir Block in the north from the deformed and uplifted Anatolide-Tauride carbonate platform in the south [*Şengör and Yılmaz*, 1981]. The northeastern part of the CAFZ follows this suture zone.

The modern first-order tectonic structures of Eastern Mediterranean (Figure 1) result from the closure of the Neotethys Ocean between 30 and 25 Ma and subsequent and ongoing collision of the Arabian plate with Eurasia along the Bitlis Zagros suture zone [*Jolivet and Faccenna*, 2000; *McQuarrie and van Hinsbergen*, 2013; *Kaymakci et al.*, 2010]. Compressional tectonics in the Eastern Anatolia contrasts with rapid back-arc extension in Western Anatolia and in the Aegean Sea, which began between 35 and 30 Ma [*Jolivet and Faccenna*, 2000]. In Central Anatolia, a N-S to NE-SW compressional stress regime persisted until the late Miocene before giving way to a extensional tectonic regime [*Özsayin et al.*, 2013].

The rate of Anatolian microplate extrusion, relative to a stable Eurasian plate, increases from 18 mm a^{-1} in the east to 25 mm a^{-1} in the west and appears to be accommodated by major transform faults. Bounding the Anatolian plate in the north, the North Anatolian fault is >1200 km long dextral strike-slip fault that stretches from the Karliova triple junction in the east before widening into the north Aegean in the west (Figure 1). With cumulative offset estimated at 85 km [*Barka et al.*, 2000], the North Anatolian fault accommodates transform motion between the Anatolian and Eurasian plates. GPS-derived slip rates of 24 ± 1 mm a^{-1} have been estimated from regional block models [*McClusky et al.*, 2000] with local estimates of 22 ± 3 mm a^{-1} at the western end of the fault [*Straub et al.*, 1997]. The North Anatolian fault formed as a result of strain localization, between 13 and 11 Ma in the east with much younger (<1 Ma) estimates of strain localization in the west [*Şengör et al.*, 2005]. Comparisons of geodetic and longer-term, geologic slip rates suggest that movement along the fault is currently faster than it has in the past [*Reilinger et al.*, 2006] and may not have formed immediately following the collision of Arabia [*Allen*, 2010].The East Anatolian fault is a 550 km long plate-bounding transform fault between the Arabian and Anatolian plates (Figure 1). Geodesy reveals that the East Anatolian fault has a modern slip rate of 9.7 ± 0.9 mm a^{-1} [*Reilinger et al.*, 2006]. Its poorly resolved total offset estimated between 8 and 30 km is much less than the North Anatolian fault [*Westaway and Arger*, 2001], resulting from both lower slip rates and later inception between 5 and 2 Ma ago [*Yilmaz et al.*, 2006]. This northeast trending left-lateral transform fault zone forms a triple junction with the North Anatolian fault in the northeast and with the Dead Sea fault zone in the southwest. The relative African-Arabian plate motions have been accommodated by the left-lateral Dead Sea fault zone at a rate of 4.5–4.8 mm a^{-1} [*Reilinger et al.*, 2006].

In addition to Arabian collision and Aegean extension, the tectonics of Central Anatolia has been influenced by the subduction of the African slab beneath Anatolia. The geochemical signature of postcollisional volcanism and geophysical estimates of lithospheric thickness in Eastern Anatolia have also led to interpretations of slab breakoff and delamination of mantle lithosphere in Eastern Anatolia sometime after 11 Ma [*Şengör et al.*, 2003; *Keskin*, 2003]. This slab break-off event beneath the Eastern Anatolian compressional province (Figure 1) has been proposed as a potential trigger for the initiation of the North Anatolian fault [*Faccenna et al.*, 2006]. Recent studies of Pn [*Gans et al.*, 2009] and *P* wave [*Biryol et al.*, 2011] tomography are consistent with the CAFZ being a major lithospheric-scale structure be the western extent of and interpretations that it may be the slab break-off event beneath Eastern Anatolia.

Early GPS studies [*McClusky et al.*, 2000; *Reilinger et al.*, 2006] found that the Anatolian plate extrudes westward away from the Arabian collision zone as a counterclockwise-rotating coherent rigid body, requiring minimal internal plate deformation. This contrasts with the geologic record, which reveals a complex history of deformation within the Anatolian plate along second-order tectonic structures such as the CAFZ [*Koçyiğit and Beyhan*, 1998; *Umhoefer et al.*, 2007; *Idleman et al.*, 2014], the Malatya-Ovacık fault zone [*Kaymakci et al.*, 2006; *Westaway et al.*, 2008], the Sürgu fault [*Koç and Kaymakcı*, 2013], and the Tüz Gölü fault zone (TGFZ) [*Çemen et al.*, 1999]. Furthermore, a review of regional paleomagnetic data shows a gradual east to west transition from counterclockwise to clockwise block rotations between smaller crustal blocks across Anatolia since 12 Ma [*Piper et al.*, 2010]. Heterogeneous deformation patterns in Central Anatolia have also been demonstrated by a recent geodetic study. *Aktuğ et al.* [2013] use a dense array (30–50 km spacing) of GPS stations that demonstrate extension rates of up to 2 mm a^{-1} and 50–100 nanostrain a^{-1} along the middle part of the CAFZ [*Aktuğ et al.*, 2013].

2.2. The Central Anatolian Fault Zone (CAFZ)

Koçyiğit and Beyhan [1998] proposed the existence of the CAFZ (Figure 2), defined as an active major intracontinental shear zone, linking a system of similarly striking, potentially interconnected faults for 730 km from the North Anatolian fault across the interior of the Anatolian plate and into the Mediterranean Sea. They suggested that it nucleated in its southern part by reactivation of the Ecemiş fault (Figure 2) and then propagated to the NE and SW to cross the entire Anatolian plate. They divided the fault system into three parts (north, central, and south) and 24 distinct fault segments that record up to 24 km left-lateral displacement since the late early Pliocene. Subsequent studies either disputed the proposed activity and continuity of the fault zone [i.e., *Westaway*, 1999; *Westaway et al.*, 2002] or focused on the kinematics and structure of individual faults [*Çetin*, 2000; *Jaffey and Robertson*, 2001; *Dirik*, 2001; *Koçyiğit and Erol*, 2001; *Jaffey et al.*, 2004; *Akyuz et al.*, 2013; *Sarıkaya et al.*, 2015b]. From SW to NE, the following active segments have

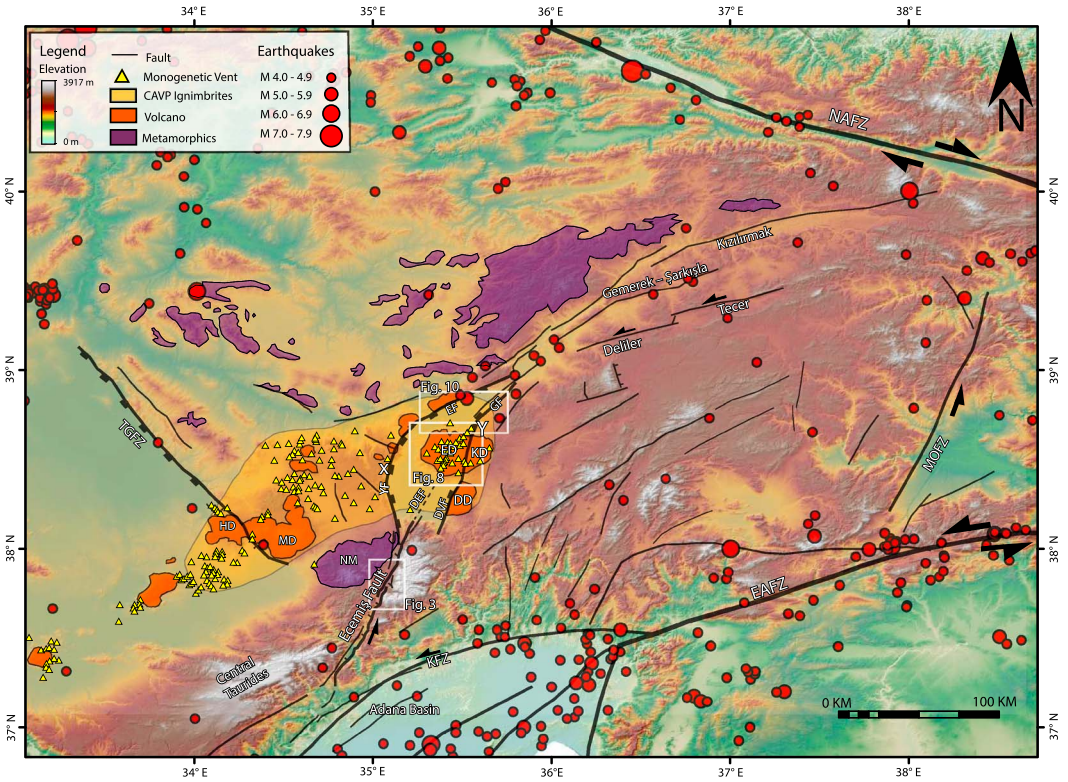

Figure 2. Composite digital elevation model and shaded relief map of Central Anatolia. The thick black lines indicate major plate boundaries NAFZ: North Anatolian fault zone and EAFZ: East Anatolian fault zone. The thin black lines represent second-order tectonic structures, CAFZ: Central Anatolian fault zone, MOFZ: Malatya Ovacık fault zone, TGFZ: Tüz Gölü fault zone KFZ: Kozan fault zone, major polygenetic volcanoes in oranges ED: Erciyes Dag, KD: Hasan Dag, DD: Develi Dag, MD: Melendiz Dag, HD: Hasan Dag, metamorphics of the Central Anatolian Crystalline Complex are in purple, including the Nigde Massif, ND along the Ecemis fault. *X* and *Z* are sinistral piercing points (28 km) proposed in *Toprak* [1998].

been verified. Two major, recently active fault strands mark the Ecemiş corridor near the town of Demirkazık [*Koçyiğit and Beyhan*, 1998, 1999]. At the eastern margin of the Ecemiş fault zone, the Cevizlik fault is a steeply west dipping mountain-front normal fault bounding the west side of the Aladağlar Range. It juxtaposes Mesozoic carbonates of the Taurides in the footwall against the Oligocene-Miocene Burç and Cukurbağ formations and overlying Quaternary alluvium in the hanging wall. The Demirkazık-Sulucaova fault runs parallel to the Cevizlik fault in the center of the valley and shows clear signs of normal and sinistral displacement.

These active fault segments comprise an array of strands that define the Ecemiş corridor, or graben, a fault zone that obliquely cuts through the more E-W striking structures of the Tauride platform. The fault was first studied by *Yetiş* [1984], who dated its main phase of activity to the Paleocene-Eocene based on biostratigraphy and inferred 80 km left-lateral displacement. *Jaffey and Robertson* [2001] proposed a similar total left-lateral Cenozoic offset of 60 km based on structural and stratigraphic evidence with most of the strike-slip displacement occurring between 13 and 5 Ma. However, they also identified a younger kinematic phase in Pliocene-Quaternary deposits, which records mostly east-west extension along the Ecemiş fault zone with a minor strike-slip component. The change in kinematics was attributed to rotation of the fault zone from NE-SW to its modern NNE-SSW orientation, which more easily accommodates the current E-W extension associated to the westward extrusion of Anatolia [*Jaffey and Robertson*, 2001].

North of the Ecemis corridor the CAFZ broadens to 30 km in the southern Erciyes extensional basin (Figure 2). The basin is bounded by the Yeşilhisar and Develi normal faults in the west and east, respectively. The Dundarlı-Erciyes fault maintains the trend of the Ecemiş fault zone through the center of the basin and continues as the Gesi fault on the north side of Erciyes Dağ stratovolcano, where it then bounds the basin in the SE. The Yeşilhisar fault bends to the NE near the town of Incesu and becomes the Erkilet fault, which bounds the basin in the NW. The center of the Erciyes basin is occupied by Mount Erciyes, the largest

stratovolcano in Central Anatolia (Figure 2), covering an area of over 555 km^2 and reaching 3917 m above sea level, nearly 3000 m above the surrounding extensional basin. Mount Erciyes developed in two stages. Construction of the Koç Dağ volcano in the eastern part of the complex culminated with caldera collapse and deposition of the regionally extensive Valibaba Tepe Ignimbrite [*Şen et al.*, 2003]. Normal faulting with a minor strike-slip component is pervasive in these older volcanic units. The second stage of volcanism (2.6 Ma to present) constructed Mount Erciyes. The slopes of the central volcano are dotted by numerous andesitic, dacitic, and basaltic lava domes, flows, and cinder cones [*Şen et al.*, 2003]. Many studies have inferred faults crossing the volcano [*Koçyiğit and Beyhan*, 1998; Kayseri sheet, *Mineral Research and Exploration General Directorate (MTA)*, 2002; *Jaffey et al.*, 2004], but the accumulation of volcanic products limits fault exposure. The Erciyes basin has been interpreted as both a releasing bend and a pull-apart basin [*Toprak*, 1998; *Koçyiğit and Erol*, 2001] with estimated offset of 28 km based on the distribution of volcanoes proposed to have been aligned prior to basin opening ([*Toprak*, 1998] *X* and *Y* in Figure 2). *Koçyiğit and Erol* [2001] suggested that the opening of the basin followed the deposition of the Valibaba Tepe Ignimbrite, while *Jaffey et al.* [2004] claimed that the most recent faulting in the Erciyes basin occurred along the sinistral Dundarlı-Erciyes fault and can be linked with late Quaternary strike-slip faulting in the Ecemiş corridor.

The northern CAFZ consists of a broad, 25–80 km wide zone stretching 200 km from north of the Erciyes basin toward the North Anatolian fault (Figure 2). It consists of dominantly strike-slip, NE trending sinistral strike-slip faults and related pull-apart basins [*Yılmaz and Yılmaz*, 2006]. From north to south, the major left-lateral structures include the Kızılırmak, Gemerek-Şarkışla, Delier, and Tecer faults (Figure 2). *Koçyiğit and Beyhan* [1998] hypothesize that these faults follow a zone of weakness along the Inner Tauride suture zone. The southernmost Tecer fault has been active during the Holocene as a slow-moving, pure strike-slip fault, with an estimated slip rate of 1 mm a^{-1} [*Akyuz et al.*, 2013].

Existing work has not demonstrated clearly the fault zone connectivity or robust offset markers, the lack of which provides the motivation for this study. We have targeted key sites where different parts of the fault zone are thought to connect or demonstrate left-lateral offset.

3. Methods

3.1. Mapping

Pliocene and Quaternary fault traces were mapped using high-resolution (50 cm) Digital Globe WV01 panchromatic and WV02 multispectral satellite imagery and Advanced Spaceborne Thermal Emission and Reflection digital topography. Kinematic data and strain markers were measured in the field on fault planes and plotted on stereonets. Fault scarp topography was surveyed in the field using a Trimble R3 GPS System. Data were projected on straight transects perpendicular to the scarps. Land surfaces were interpolated from elevation points on either side of the fault scarps. To calculate throw and extension, fault angle was measured in the field, and the fault plane was assumed to intersect the ground surface at the midpoint of the fault scarp.

3.2. Volcanic Geomorphology

Linear arrays of vents are common in monogenetic volcanic fields, when multiple vents are sourced from the same magma feeding dike. Dikes are often in line with the principal compressive stress ([*Rubin*, 1995] World Stress Map Project [*Heidbach et al.*, 2001]) and perpendicular to the minimum principal stress (σ_3) [*Paulsen and Wilson*, 2010; *Le Corvec et al.*, 2013]. We employ the azimuth methods of *Cebriá et al.* [2011] for statistical identification of meaningful vent alignments. Local-scale alignments are identified statistically by considering mean intervent distance (X) and standard deviation (σ) for the entire field. We find that preferred orientations are best identified when considering vents within the lower half of the anomalously short distances (i.e., $d \leq (x - \sigma)/2$). Best fit lines of the center points are determined by linear regression and define the alignments azimuth and length.

3.3. Geochronology

3.3.1. Cosmogenic ^{36}Cl Dating

We combine geomorphic analysis of offset fan and terrace surfaces in the Ecemiş corridor with terrestrial cosmogenic nuclide exposure dating [*Gosse and Phillips*, 2001; *Gosse*, 2011] to estimate prehistoric slip rates.

Table 1. Sample Characteristics and Geochemical and Isotopic Analytical Data for Sample From Ecemiş Fault Zone

Sample No.[a]	Thickness[b]	Latitude (°N)[c]	Longitude (°E)[c]	Elevation (m)[d]	Shielding[e]	Major Elements (wt %)[f]											Trace Elements (ppm)[g]					
						Al_2O_3	CaO	Fe_2O^3	K_2O	MgO	MnO	Na_2O	P_2O_5	SiO_2	TiO	CO_2	Cl[h]	B	Sm	Gd	U	Th
TIC-02a	3 cm	37.50	35.05	1759	0.997	0.04	55.2	0.03	0	0.33	0	0	0	0.06	0	43.6	36.6	0	0.2	0.28	0.23	0.3
TIC-02b	3 cm	37.50	35.05	1759	0.997	0.05	54.8	0.02	0	0.47	0	0.03	0.02	0.13	0	43.9	53.0	0	0.1	0.06	0.16	0.2
TIC-02d	3 cm	37.50	35.05	1759	0.997	0.07	54.9	0.07	0	0.36	0	0.01	0.02	0.12	0	43.8	48.9	0	0.3	0.29	0.26	0.2
TIC-06b	3 cm	37.85	35.07	1605	0.998	0.06	55.3	0	0	0.23	0	0.02	0	0.17	0	43.5	21.9	0	0.2	0.29	0.22	0.1
TIC-06c	3 cm	37.85	35.07	1609	0.998	0.04	55.8	0.04	0	0.34	0	0.03	0	0.19	0	42.9	43.4	0	0	0	0.18	0
TIC-06e	3 cm	37.85	35.07	1609	0.998	0.04	55	0	0	0.32	0	0.02	0.02	0.11	0	43.8	26.9	0	0.2	0.23	0.14	0
TIC-06f	3 cm	37.85	35.07	1609	0.998	0.04	55.1	0.03	0	0.33	0	0.02	0.01	0.21	0	43.5	26.5	0	0.1	0.08	0.14	0

[a]Water content assumed at 0.05 wt %.
[b]Average sample depth used for thickness correction.
[c]Decimal degrees, from handheld GPS ± 5 m.
[d]Decimal degrees, from handheld GPS ± 15 m.
[e]Calculated from 30° measurements of the inclination to the horizon using a handheld clinometer.
[f]Major element concentration detection limits are 0.01%.
[g]Trace element detection limits are 0.1 ppm.
[h]The $^{36}Cl/Cl$(total) ratio measured with AMS on spiked samples and converted back to original rock values.

The lack of large boulders on the surface and the presence of a >2 m thick petrocalcic horizon in the shallow surface caused us to use surface cobbles for modern dating the fan surface. We collected cobbles from the well-cemented calcrete surfaces of an alluvial fan (three cobbles) and of a fluvial terrace (four cobbles). These well-rounded cobbles range from 10 to 15 cm in diameter. We selected only samples that were stable within the cemented surface, extracted from calcrete exposed through variably thick soil and regolith. Low surface slopes and high degree of cementation indicate that the cobbles have not been moved or otherwise disturbed since emplacement.

To date the emplacement of the cobbles within the alluvial units we used in situ-produced ^{36}Cl generated within the limestone and marble clasts. The limestone cobbles were cleaned of pedogenic carbonate by chipping and leaching in dilute HNO_3 acid, then dried, crushed, and sieved. Approximately 29 g of the 355–500 μm fraction of single-cobble samples were prepared at the Dalhousie Geochronology Centre according to the carbonate methodology of *Stone et al.* [1996]. Approximately 1.8 mg of Cl spike prepared from an Oak Ridge National Laboratory Cl salt with $^{35}Cl/^{37}Cl$ ratio of 0.999 was added to each sample. The $^{36}Cl/Cl_T$ and $^{35}Cl/^{37}Cl$ were measured by accelerated mass spectrometer at Purdue Rare Isotope Measurement Laboratory, Purdue University, against standard SRM4943. Accelerator mass spectrometry (AMS) 1σ precision was between 2 and 4% for the samples, and the process blank yielded a ratio 2 orders of magnitude less than values measured in the samples. Major elements were measured by XRF, and selected trace elements were measured by inductively coupled plasma–mass spectrometry at SGS Mineral Services in Lakefield, Ontario, with 5% (1σ) precision. Over 95% of in situ ^{36}Cl in our limestone samples was produced from spallation from Ca. Data reduction followed the procedure by *Marrero* [2012], with calibrated ^{36}Cl production rates according to *Marrero* [2012] and scaling according to *Lifton et al.* [2014]. Ages were computed by the ^{36}Cl CRONUS-Earth online calculator Web calculator v. 1.0 accessed in August 2015 (Cosmic-Ray Produced Nuclide

Table 2. ^{36}Cl Cosmogenic Isotope Data, Production Rates, and Mean Surface Ages

Sample ID		^{36}Cl Cosmogenic (10^4 atoms g^{-1} sample^{-1})	^{36}Cl Cosmogenic (atoms g^{-1} sample^{-1})	Production Rate[a] (atoms g^{-1} yr^{-1})	^{36}Cl Cobble Age[b] No Erosion	^{36}Cl Cobble Age[b] 7 mm ka^{-1}	^{36}Cl Cobble Age[b] 7 mm ka^{-1} Inheritance Correction[d]	Surface Age[c] No Erosion	Surface Age[c] 7 mm ka^{-1}	Surface Age[c] 7 mm ka^{-1} Inheritance Correction[d]
TIIC-02a	QAF-1	819 ± 40	8192876	63.7	100 ± 10 ka	108 ± 12 ka	104 ± 12 ka	97.5 ± 10 ka	105 ± 15 ka	98.6 ± 13 ka
TIIC-02b		775 ± 37	7752707	63.7	93 ± 9.5 ka	102 11 ka	92 ± 11 ka			
TIIC-02d		830 ± 38	8295015	63.7	94.1 ± 9.6 ka	110 ± 12 ka	101 ± 12 ka			
TIIC-06b	QFT-1	326 ± 16	3257284	54.0	45.6 ± 4.6 ka	48 ± 5.5 ka	48.2 ± 5.5 ka	42.9 ± 4.4 ka	44.5 ± 4.6 ka	40.3 ± 4.0 ka
TIIC-06c		325 ± 14	3245276	55.0	43.4 ± 3.9 ka	47 ± 5.0 ka	38.1.8 ± 3.6 ka			
TIIC-06e		288 ± 19	2879095	53.7	40.5 ± 3.9 ka	42 ± 4.6 ka	42.0 ± 4.3 ka			
TIIC-06f		308 ± 13	3079791	53.9	43 ± 3.9 ka	45 ± 4.6 ka	37.9 ± 3.6 ka			

[a]Total production rate of ^{36}Cl over the total sample thickness.
[b]Uncertainties given at 1σ and calculated by AMS reported analytical error on ^{36}Cl/Cl ratio.
[c]Weighted average of cobble ages with uncertainties. Weighted mean uncertainties are analytical, as they were greater than the error due to the spread of the data.
[d]Inheritance corrected using inherited component of ^{36}Cl reported in *Sarıkaya et al.* [2015b].

Systematics on Earth: http://web1.ittc.ku.edu:8888/). All essential sample information to calculate the ages is provided in Tables 1 and 2.

3.3.2. ^{40}Ar/^{39}Ar Dating

Additional age constraints on faulting were provided by dating of five volcanic samples, including lava flows, monogenetic volcanoes, and welded ignimbrite flows. Samples were selected from unweathered interiors of outcrops. ^{40}Ar/^{39}Ar analyses were completed at U.S. Geological Survey (USGS) in Denver, Colorado (two analyses) and University of British Columbia in Vancouver, Canada (three analyses). We use a combination of incremental heating experiments of whole rock (three samples) and amphibole (one sample) and individually fused plagioclase grains (one sample). Initial data entry and calculations were carried out using the software ArArCalc [*Koppers*, 2002]. The plateau and correlation ages were calculated using Isoplot v. 3.09 [*Ludwig*, 2003]. Errors are quoted at the 2 sigma (95% confidence) level and are propagated from all sources except mass spectrometer sensitivity and age of the flux monitor. Additional details are given in the supporting information.

4. Site Analysis

Results and implications are presented from south to north.

4.1. Site 1 Ecemiş Corridor

The steeply dipping, range-front, Cevizlik fault scarp (Figure 3) is several hundred meters high in places, and the fault has ruptured late-Quaternary colluvium (Figure 4a) with minimal normal displacements (<1 m; Figure 4b). The Cevizlik fault can be traced sporadically along the entire length of the Ecemiş corridor. The Demirkazık-Sulucaova fault has a narrow (10–50 m), linear N25°E trending oblique strike-slip trace located in the center of the Ecemiş valley, with a length of 19.1 km. Shutter ridges, elongated hills, and deflected and offset stream courses are found along its trace, providing evidence of recent left-lateral displacement on the Demirkazık-Sulucaova fault. The main east dipping fault scarp is well exposed in a stream cut south of Pınarbaşı, where it dips 65° and displaces both Oligocene-Miocene sediments and a Quaternary alluvial fan surface. A series of fluvial terraces bury the Demirkazık-Sulucaova fault in several locations and present an ideal site to constrain short-term slip rates.

4.1.1. Geomorphic Surfaces

Alluvial fans in the study area are extensive in plan view, have wedge-shaped geometries, and are fed from both the Yaluk and Emli River drainages (Figure 3). Away from the mountain front, slopes shallow to 3–4° in the middle and distal parts of the fan. The basal, texturally

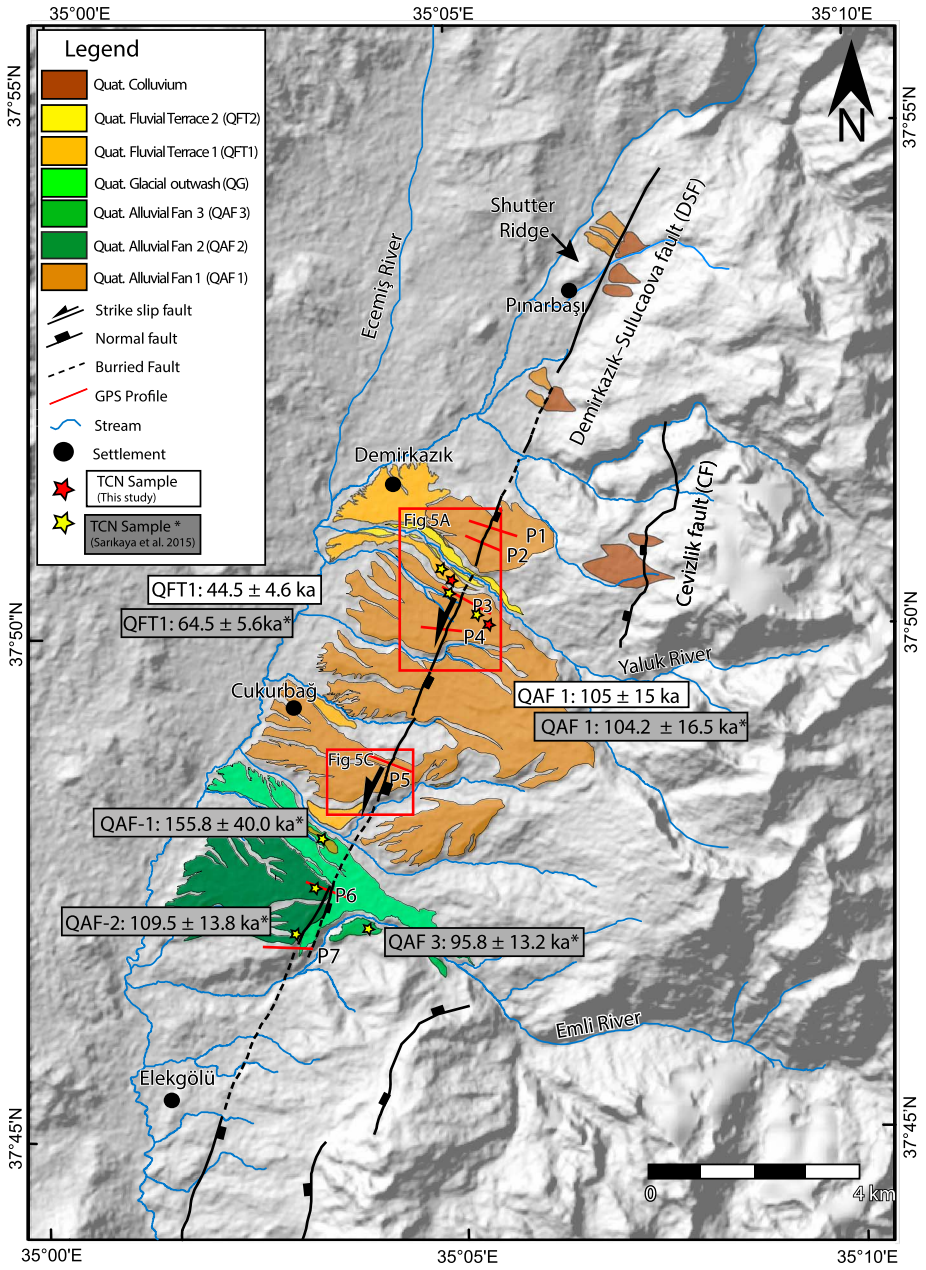

Figure 3. Hillshade base map with a Quaternary geomorphic map of the northern Ecemiş fault zone. Ages presented are from this study (QAF-1 and QFT-1) and *Sarıkaya et al.* [2015a, 2015b] (QAF-1,QAF-2, and QAF-3).

immature clastic intervals of the fan deposits are interpreted as high-energy debris flows formed in response to steep slopes created by mountain-front extensional faulting on the Cevizlik fault [*Jaffey and Robertson*, 2005]. Paleocurrent trends within the fan deposits show flow direction perpendicular to the mountain front. The Quaternary alluvial fan units (QAF-1 to QAF-3) unconformably overlie the heavily deformed Miocene Burç and Cukurbağ formations. Statigraphically higher depositional units within the fans are more texturally mature, displaying imbrication, good sorting, and strong lamination in distal parts of the fan (Figure 4d). The conglomerates are monogenetic and coarse grained, comprising well-rounded to subrounded pebble to cobble-sized clasts sourced almost entirely from the Jurassic limestones of the Aladağlar Range. The upper surface is well cemented by calcrete. The capping lithified horizon increases in thickness from 4 to 5 m in the distal parts of fan. The surface is generally low relief and well preserved, although thin regolith and localized incision of up to 30 cm is not uncommon. Similar "fossilized" geomorphic surfaces have been described in

Figure 4. Field photos from the Ecemiş fault zone. (a) Mountain front Cevizlik fault. (b) Cevizlik fault rupture of Quaternary Colluvium. (c) South looking view at the east dipping oblique Demirkazık-Sulucaova fault (DSF). (d) Profile view of the distal part of the calcrete encased Quaternary alluvial fan (QAF-1). (e) Representative sample of cobble sampled from QFT 1. Representative sample of cobbles sampled from QAF-1.

SE Spain by *Stokes et al.* [2007], who attributed calcrete development to a combination of pedogenic and groundwater processes. Over time, calcrete encasement of these surfaces increases, stabilizing the surfaces and protecting them from erosion.

Three levels of abandoned river terraces stand 5 (QFT-3), 10 (QFT-2), and 20 m (QFT-1) above the Yaluk stream (Figure 5b). Their deposits are made of well-sorted conglomerates and gravels, composed of rounded limestone clasts 1 to 15 cm in diameter. The degree of cementation of the calcrete horizon capping these surfaces increases with height (and inferred age) of the abandoned terraces. The youngest (lower) fluvial terraces are unconsolidated at the surface, while the oldest fluvial terrace (QFT-1) has a well-cemented horizon down to a maximum depth of 1 m. Similar surfaces are deeply incised along the Emli River and are described in detail by *Sarıkaya et al.* [2015a, 2015b]. At both localities, these surfaces are undeformed where they cross the Demirkazık-Sulucaova fault and record no vertical or horizontal offset (Figure 5b).

4.1.2. Displacement

Alluvial fans in active tectonic settings can provide excellent piercing points to constrain offset, where recently active faults displace streams or terrace risers. Interpretation of these geomorphic landforms can be complex, and careful consideration of multiple piercing points and their reliability is required for accurate slip rate estimates [*Cowgill*, 2007]. Deflected and beheaded streams, offset terrace risers,

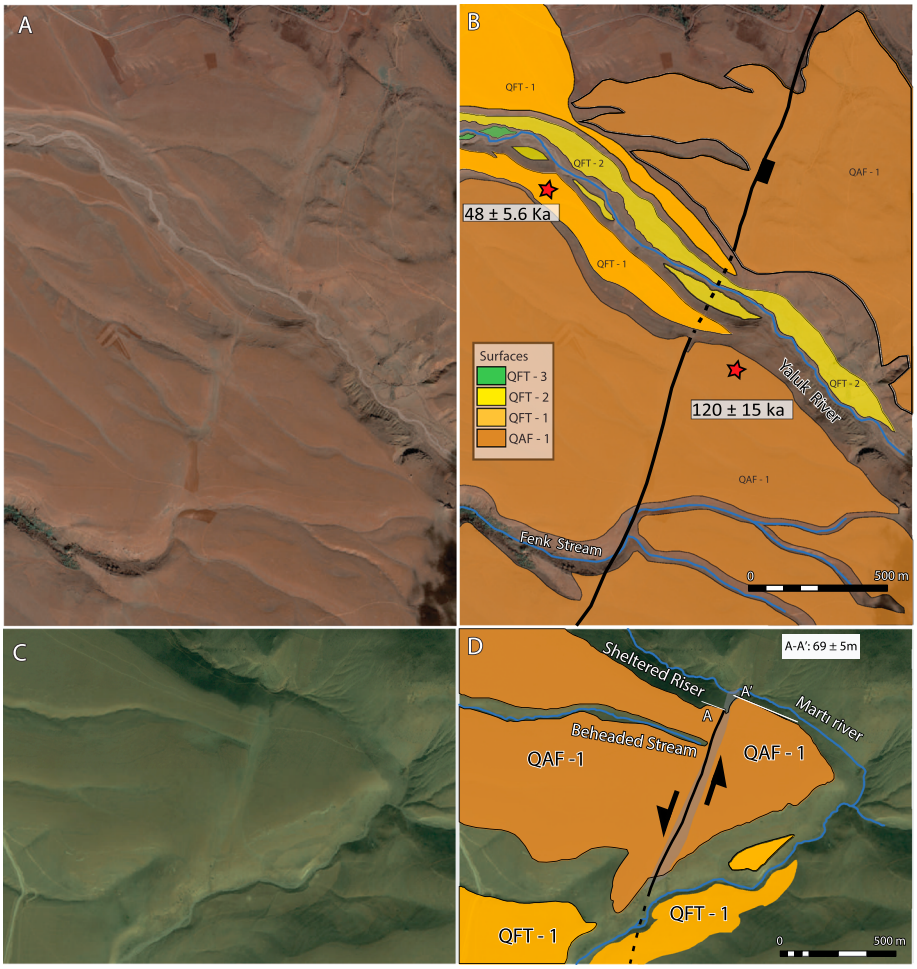

Figure 5. (a) Close ups of faulted and unfaulted geomorphic surfaces along the Yaluk Stream. (b) Interpreted with surfaces with ^{36}Cl sample locations. (c) Uninterpreted view of the alluvial fan surface near Cukurbag. (d) Interpreted piercing points from the same surface. Copyright Digital Globe.

and shutter ridges record strong evidence for sinistral displacement of the QAF-1 surface along the 19.1 km trace of the Demirkazık-Sulucaova fault. However, the study area highlights many of the complexities associated with offset geomorphic landforms; previous studies have arrived at very different geomorphic interpretations and estimates of late-Quaternary horizontal offset.

Koçyiğit and Beyhan [1999] cite 70 m of sinistral displacement of QAF-1 along the Demirkazık-Sulucaova fault, although their piercing point is not explicitly documented. *Jaffey and Robertson* [2001] argue that for a minimum offset of 250 m of QAF-1 based on left-lateral deflection of the Fenk stream (Figure 5c). *Sarıkaya et al.* [2015b] challenge this estimate, pointing out that the geometry of the east dipping Demirkazık-Sulucaova fault creates a barrier to streams flowing west from the Aladağlar Range. Low-order streams without sufficient hydrological power to overcome the topographic barrier are deflected along the fault scarp and may appear as left-lateral offsets. Instead, *Sarıkaya et al.* [2015b] prefer a value of 168 ± 2 m based on a reconstruction of the offset terrace riser immediately to the north of the Yaluk stream (Figure 5b).

We focused on the best preserved offset markers near Çukurbağ (Figure 5d; see Figure 3 for location), where the terrace riser south of the Martı River is steeply incised and displaced (Figure 5d). Following displacement the terrace riser located west of the fault (A in Figure 5d) was sheltered from incision and therefore presents the clearest and best preserved evidence of recent left-lateral faulting. Lateral offset of QAF-1 was measured from piercing points on high-resolution satellite imagery. To reconstruct total fault offset we projected both risers toward the fault, estimating 69 ± 5 m of left-lateral displacement (A-A'; Figure 5d). We presume this to be the same offset cited by *Koçyiğit and Beyhan* [1999].

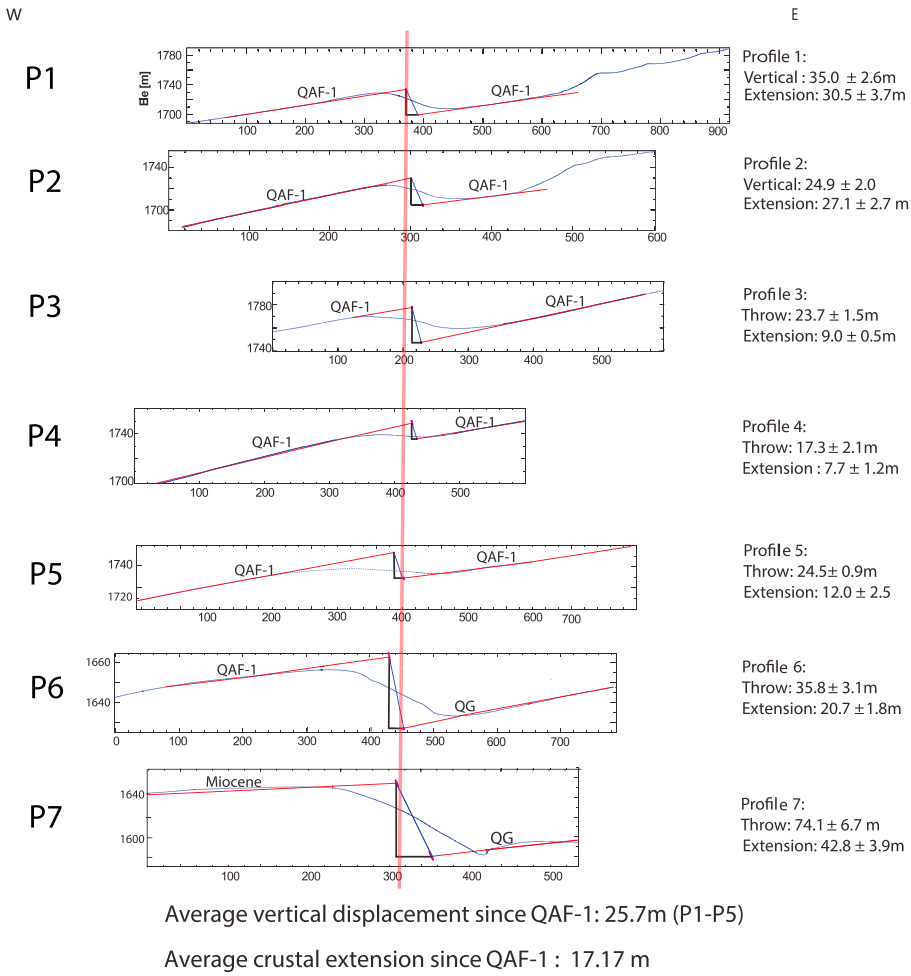

Figure 6. Topographic profiles used to constrain normal offset of the Demirkazık–Sulucaova fault. Geomorphic surface slopes and a field observed fault angle of 65° are used to reconstruct original fault geometry and calculate both throw and extension. See Figure 3 for profile locations.

Vertical displacement was constrained using six GPS profiles across the Demirkazık-Sulucaova fault scarp (Figure 6). Normal displacement across the east dipping fault in profiles 1 to 6 averages 25.7 ± 3 m, resulting in an approximately 3:1 ratio for strike-slip versus dip-slip displacement. Offset predating the deposition of the QAF-1 is evident in profile 7, where the fault scarp offsets deformed Miocene sediments, which are draped by QFT-1 deposits. Cumulative offset recorded here is 74 ± 7 m.

4.1.3. ^{36}Cl Exposure Ages of Geomorphic Surfaces

We dated the QAF-1 and QFT-1 surfaces along the Yaluk River using cosmogenic ^{36}Cl exposure dating of surface cobbles. Sample characteristics and compositional data are listed in Table 1. As the pedogenic carbonate horizon—which formed at depth—is now exposed at the QAF-1 and QFT-1 surfaces (Figures 4e and 4f), we must account for erosion of the overlying soil cover. An empirical study by *Royer* [1999] showed that depth to the top of pedogenic carbonate horizons is $<$1 m in 95% of cases studied. Field observations also show relief of noncemented gravel up 30 cm on the QAF-1 surface. This indicates that the cobbles imbedded in the petrocalcic horizon were previously covered by at least 30 cm. While episodic erosion cannot be excluded, we assume a gradual and constant surface erosion rate that, depending on exposure age, will account for 0 to $>$50 cm of total erosion. We report ^{36}Cl ages assuming erosion rates of 0 and 7 mm ka^{-1} (Table 2 and Figure 7). Given the age of our surfaces, 7 mm ka^{-1} erosion rates allow for removal of as much as 60 cm from QAF-1, a maximum amount of erosion we would expect at this site, and sufficient to exhume pedogenic carbonate layers. We observed no indication of sediment aggradation after formation of the main petrocalcic horizon. The lack of aggradation is reasonable considering the depth of incision of these fans, which would

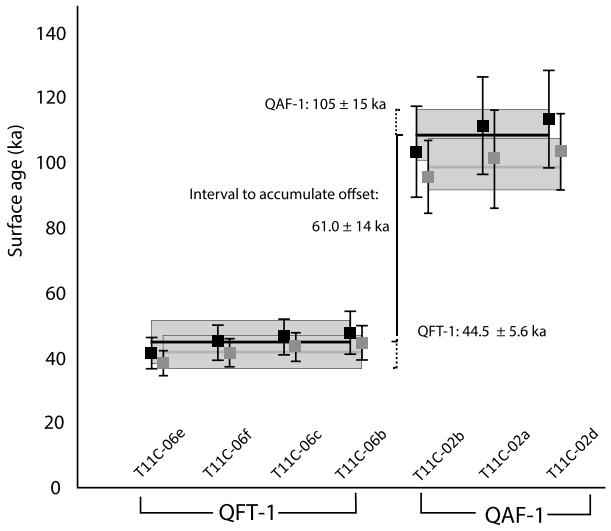

Figure 7. ^{36}Cl ages for cobble samples from the QAF-1 and QFT-1 surfaces. The black squares are ages corrected for erosion, and the orange squares are uncorrected for erosion. The horizontal black lines indicate the weighted mean age for each surface with grey boxes indicating the surface uncertainty. Time intervals between the two surfaces were used to calculate Demirkazik-Sulucaova fault slip rates.

have caused the stream to abandon the surfaces. Thus, we have only considered surface erosion in our age calculation.

Sarıkaya et al. [2015a, 2015b] identified and dated the same geomorphic surfaces (QAF-1 and QFT-1) along with two alluvial fan surfaces along the Emli River (QAF-2 and QAF-3 in Figure 3). Their study used ^{36}Cl dating of surficial samples (cobbles and boulders) and a 2.6 m depth profile in the QFT-1 surface. Their depth profile revealed an inherited component of 49.6×10^4 atoms ^{36}Cl g^{-1}, and this inheritance correction was also applied to their QAF-1 age. Their ages were scaled using the model of *Desilets and Zreda* [2003], which we found to produce ages 1 to 3% younger than our preferred time-dependent scaling methods from *Lifton et al.* [2014].

The three cobbles (TIIC-02a, TIIC-02b, and TIIC-02d) from the QAF-1 surface (Figures 3 and 5) show a strong cluster, with ages of 100 ± 10, 93 ± 9.5, and 94.1 ± 9.6 ka (Table 2; 1σ total external uncertainty). The surface has a weighted average age of 97.5 ± 10 ka. When corrected for 7 mm ka^{-1} erosion rate (Figure 7), our data give a weighted average age of 105 ± 15 ka with a 4.4% coefficient of variation (Table 2). The 7 mm ka^{-1} erosion rate increases the mean age calculated for the QAF-1 by 7.7% from the zero erosion age. However, the coefficient of variation about the mean ages of the individual cobbles from the QAF-1 surface (4.4%) is less than the total precision of each age (>10% 1σ). This suggests that the inherited ^{36}Cl concentration is either very low or very consistent, as it is unlikely that three cobbles would yield such similar ages if inheritance was significant. We favor the former, simpler interpretation because for a low inheritance catchment erosion rate must be relatively high; a high erosion rate is consistent with the observation that catchments and valleys in Aladağlar Range were glaciated during late Pleisotocene-Holocene time [*Zreda et al.*, 2011]. However, we also make a correction for inheritance using in recently published data from *Sarıkaya et al.* [2015b] that are included in Table 2. When corrected for erosion, the 7 mm ka^{-1} surface age decreases to 98.6 ± 13 ka (or ~6%).

The four cobble samples (TIIC-06b, TIIC-06c, TIIC-06e, and TIIC-06f) analyzed from the QFT-1 surface (Figures 3 and 5) yielded younger ages than the QAF surface: 48.2 ± 5.5, 44.6 ± 4.3, 42 ± 4.3, and 44.8 ± 4.4 ka (1σ total uncertainty) corrected for 7 mm ka^{-1} of erosion, yielding a weighted average ages of 44.5 ± 4.6 ka (43.0 ± 4.4 ka with zero erosion). Like the QAF-1 surface, the ages have a low coefficient of variation about their mean (5.0%).When corrected for erosion, the 7 mm ka^{-1} surface age decreases to 40.3 ± 4.0 ka (or ~9%).

When the different data sets are treated the same way (*Desilets and Zreda*'s [2003] scaling, corrected for inheritance; 7 mm ka^{-1}) our surfaces have average ages of 95.8 ± 12 ka (QAF-1) and 39.7 ± 16 ka (QFT-1) compared with ages of the 104.2 ± 16.5 ka (QAF-1) and 64.5 ± 5.6 ka (QFT-1) reported from *Sarıkaya et al.* [2015b]. We proceed in slip-rate calculations with our exposure ages of 105 ± 15 (QAF-1) and 44.5 ± 4.6 ka (QFT-1), based on our own production rates using the scaling method of *Lifton et al.* [2014] and an erosion rate of 7 mm ka^{-1} (Table 2).

4.2. Site 2: Dundarlı-Erciyes Fault

The Dundarlı-Erciyes fault trends N25°E north of the Ecemiş corridor and probably continues beneath the southern Erciyes basin (Figure 2). The fault has acted as a conduit for numerous dacitic lava domes but is buried beneath the peak of the Erciyes stratovolcano (Figure 8). At least 75 monogenetic volcanic vents

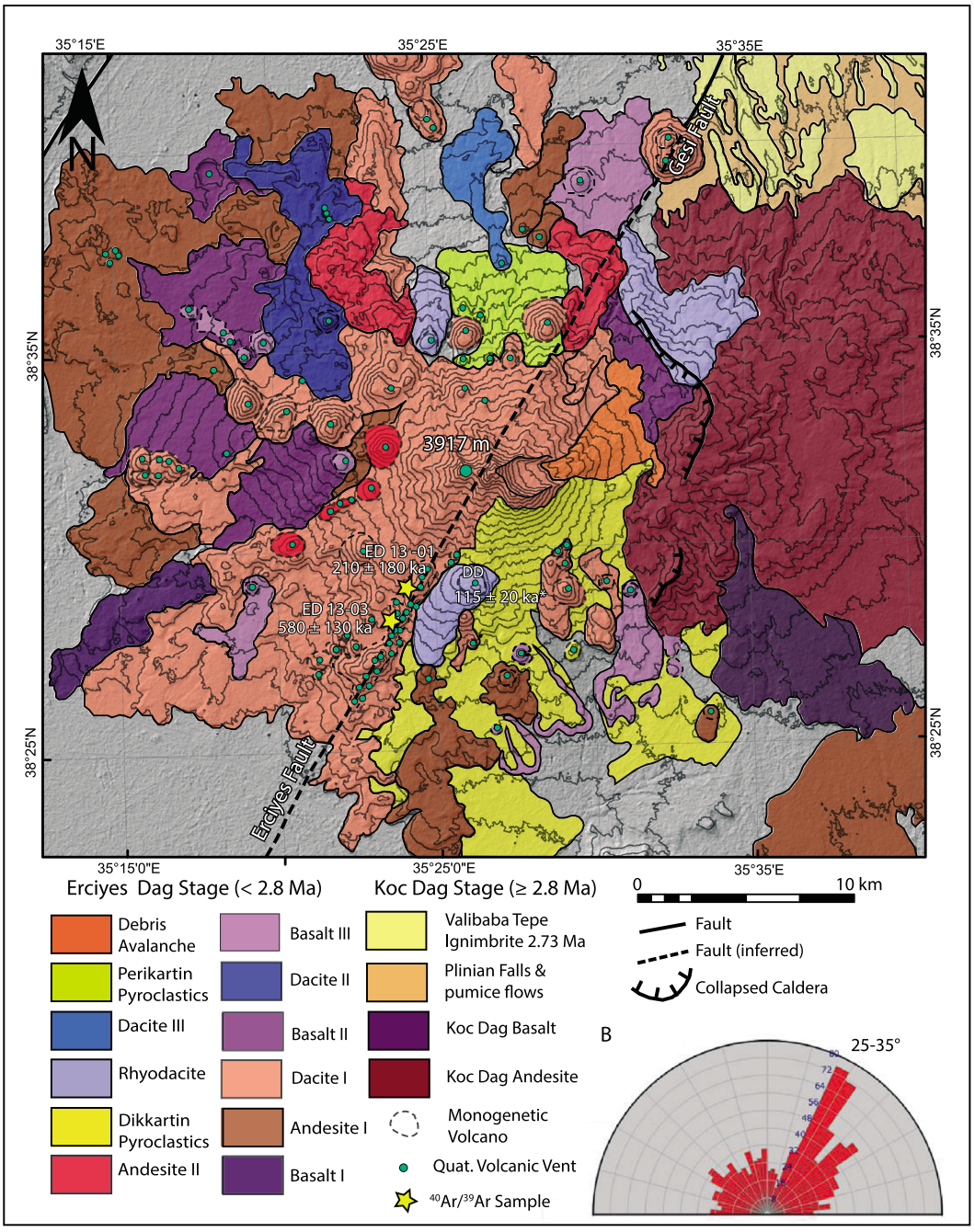

Figure 8. (a) Geologic map of the Erciyes stratovolcano on 50 m contour intervals and a shaded relief map, modified from *Şen et al.* [2003]. Samples and age data from this study and for Dikkartin Dağ (DD) from *Ercan et al.* [1994]. (b) Vent to vent azimuths for vents within 2.86 km.

are distributed on the volcano flanks. Twelve of these are basaltic cinder cones and 63 are lava domes, mostly rhyolitic and dacitic in composition. Alignments of monogenetic vents radiate out from the central peak, particularly to the west. On the SW flank of the volcano a series of volumetrically small dacitic-rhyodacitic lava domes are tightly aligned (Figure 8). The alignment has deflected the course of a younger dacite flow, erupted from Dikkartin Dağ (Figure 8), dated to 0.115 ± 0.02 Ma [*Ercan et al.*, 1994].

In the absence of fault surface ruptures through the southern Erciyes basin and the Erciyes volcanic complex, we use the alignment of volcanic vents to infer syneruptive stresses along this buried portion of the CAFZ.

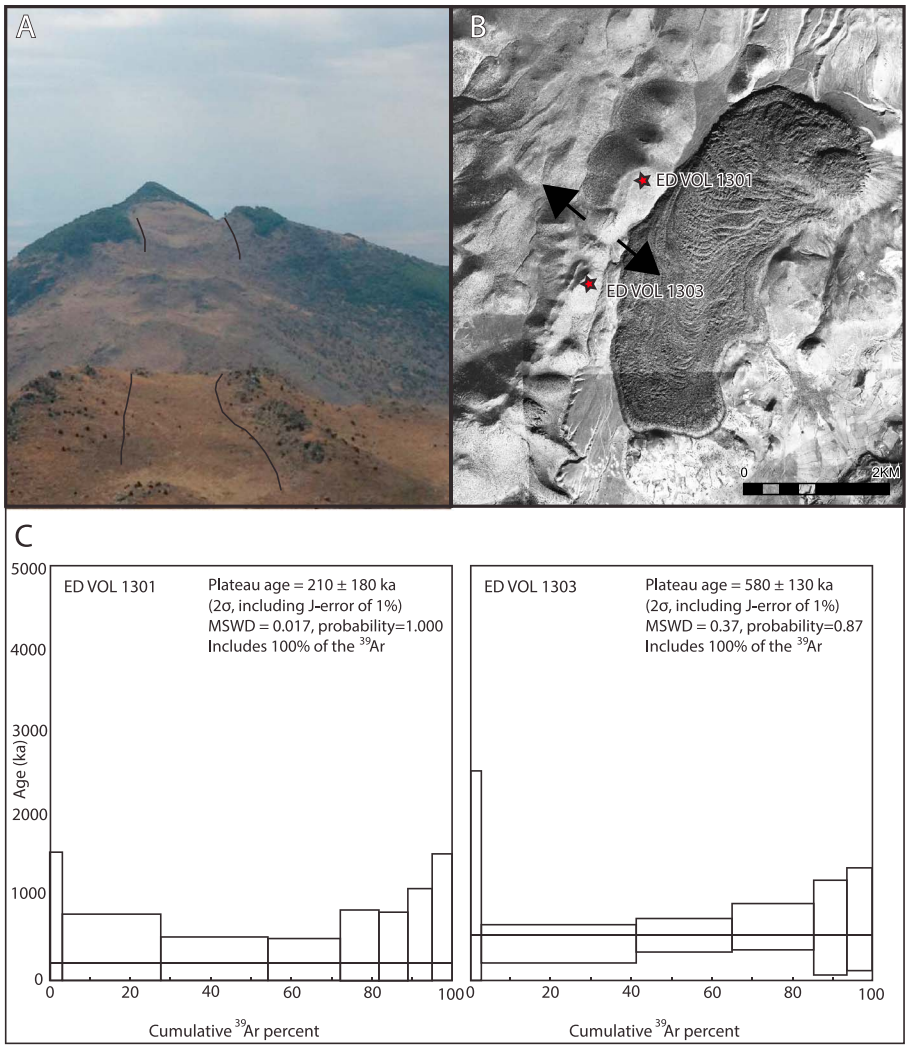

Figure 9. (a) SW view from the ED VOL 13–01 sample location looking down the vent alignment at ED VOL 1303. (b) Satellite Image of the rifted vent alignment and sample locations. Copyright Digital Globe. (c) $^{40}Ar/^{39}Ar$ results for Erciyes volcanic samples.

When we consider anomalously close vents ($d \leq (X - \sigma)/2$ or 2.86 km), a dominant azimuth direction of 25 to 35° points to an anomalous high-frequency cluster on the SW flank, where the Dundarlı-Erciyes fault is expected to cross through the stratovolcano. Fifteen individual volcanic vents are aligned above the projection of the Dundarlı-Erciyes fault. Homogeneous lithology, spatter ramparts parallel to the alignment and tight vent-to-vent spacing of between 200 and 500 m indicate that the eruptions were controlled by a fracture with low confining pressure or an extensional fault [*Corazzato and Tibaldi*, 2006; *Paulsen and Wilson*, 2010]. The alignment azimuth of N32°E indicates extension in a WNW-ESE direction along the NNE trending fault [*Nakamura*, 1977; *Paulsen and Wilson*, 2010]. Two samples from the aligned dacite domes (Figure 9b) were collected for $^{40}Ar/^{39}Ar$ dating. They are grey porphyritic dacites with 1–3 mm quartz, feldspar, and hornblende phenocrysts. $^{40}Ar/^{39}Ar$ dating of the groundmass yielded ages of 210 ± 18 ka (Erciyes Dag (ED) 13–01) and 580 ± 130 ka (ED 13–03) (Figure 9c). As geomorphic markers, these domes record no strike-slip offset since emplacement.

4.3. Site 3: Erkilet and Gesi Faults

North of the Erciyes stratovolcano the CAFZ continues to bound the Erciyes basin (Figure 10a) and offset flat-lying volcanics of the Central Anatolian volcanic province. Relief from the floor of the Erciyes depression to the surrounding plateaus is 400 to 500 m.

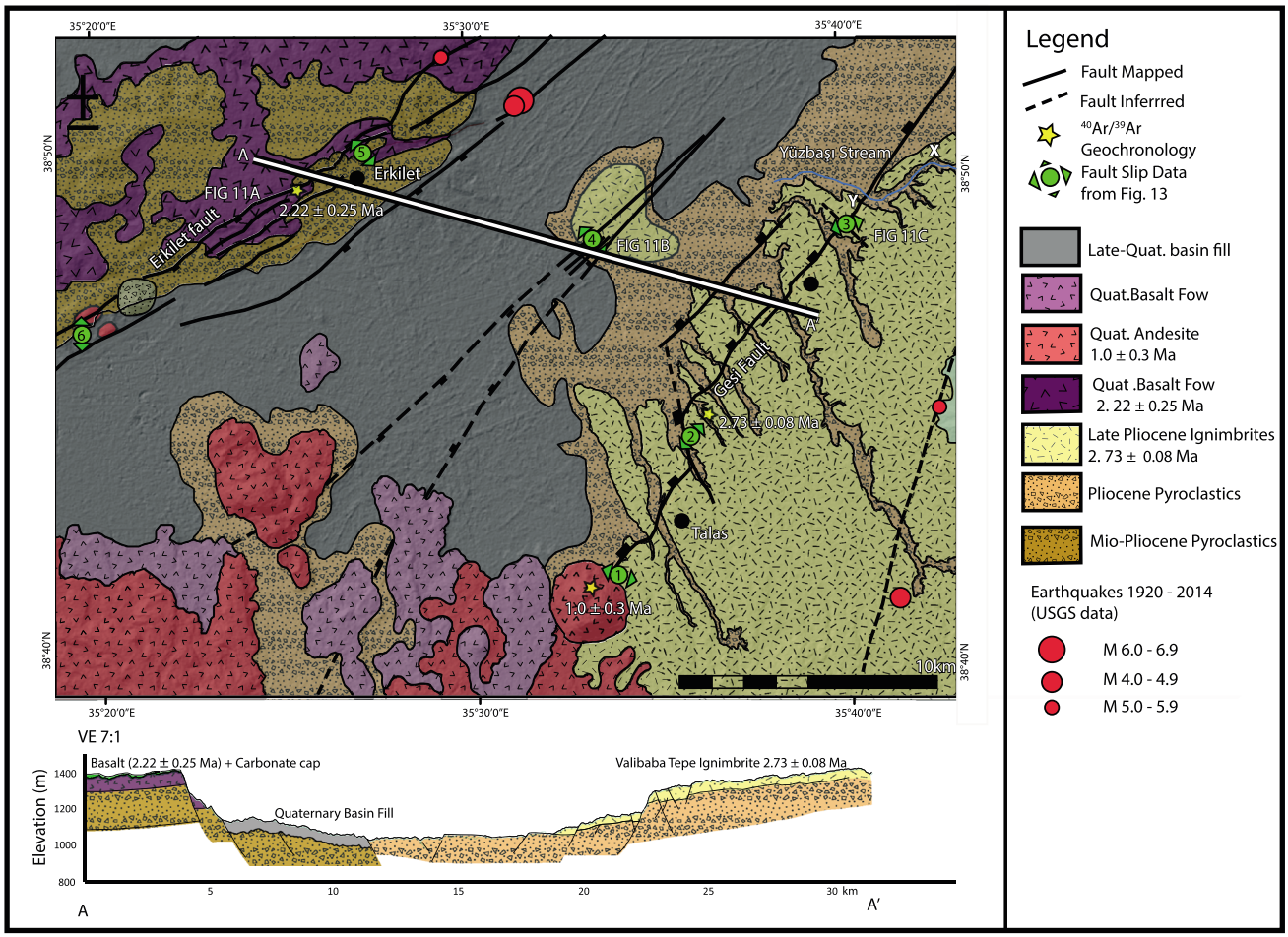

Figure 10. (a) Geologic map of the northern Erciyes basin. The yellow stars denote $^{40}Ar/^{39}Ar$ geochronology samples. Modified from Kayseri sheet, *MTA* [2002]; (b) cross section.

The Gesi fault makes up the northeast margin of the Erciyes basin, trending N30°E for 30–35 km through the towns of Talas and Gesi (Figure 10a). It juxtaposes the Valibaba Tepe Ignimbrite in its hanging wall against older pyroclastics in its footwall. The trace of the fault is generally linear, with one major left step linked by a NNE-SSW trending pure normal fault. At multiple locations, syndepositional faulting is seen in the Plinian deposits underlying the Valibaba Tepe Ignimbrite (Figure 11), which shows that activity along the Gesi fault began before emplacement of the Valibaba Tepe Ignimbrite, which yielded an $^{40}Ar/^{39}Ar$ date of 2.73 ± 0.08 Ma on plagioclase phenocrysts ($n = 10$) (T11V02; Figure 12c). The Gesi fault terminates at its southern end beneath the Ali Dağ volcanic dome, an endogenic lava dome of andesitic composition. The Gesi fault plane acted as a conduit for its emplacement. The lava dome does not exhibit any vertical or horizontal offset. Its cooling age is 1.0 ± 0.3 Ma, determined from $^{40}Ar/^{39}Ar$ dating of amphibole phenocrysts (11TR-08; Figure 12b), thus providing a minimum age for the end of activity along the Gesi fault. Our topographic surveys show that cumulative displacement on the Gesi fault reaches 230 m near Talas in the SW and decreases along strike to 130 m near Gesi in the northeast. Near the town of Gesi (Figure 11c), the exposed main fault scarp has been produced by a steep 80° west dipping fault, trending N25°E. Displacement vectors (Figure 13c) show sinistral-normal strain, with a rake of 45° to the fault plane, suggesting a small component of left-lateral motion along the Gesi fault. N-S trending antithetic normal faults (Figure 11c) dipping 60° toward the east are abundant and produce a horst-and-graben structure just east of the main strand.

The Erkilet fault bounds the Erciyes basin to the northwest; it extends over 35–40 km in a N45°E direction from SW of Erkilet to the Tuzla Gölü (Figures 2 and 10). The fault juxtaposes a flat-lying lacustrine carbonate unit and underlying horizontal basalt flow in the hanging wall with a thick volcaniclastic sequence in the footwall, made up of weakly deformed tuffs and pumice deposits. A basalt flow, with a groundmass dated to 2.22 ± 0.25 Ma

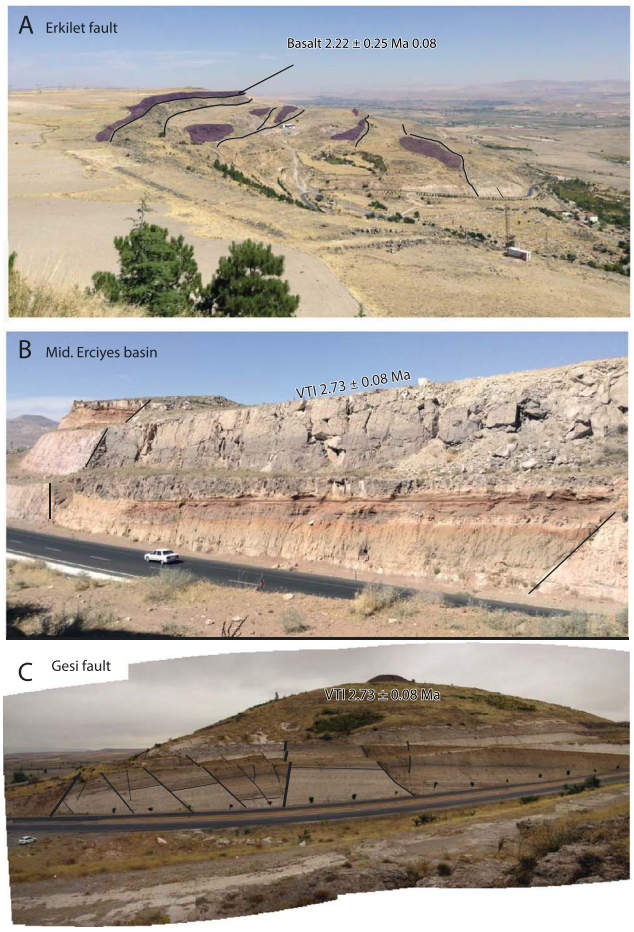

Figure 11. Field photos from the northern Erciyes basin, see Figure 10 for photo locations. (a) Downthrown basalt and step-like faulting pattern along the Erkilet fault. (b) Graben structures in the central Erciyes basin. (c) Main fault scarp and antithetic faults along the Gesi fault.

(ERK VOL-1307: Figure 12a), is exposed on both sides of the main fault and is downthrown >40 m to the basin floor in a step-like morphotectonic pattern where relay ramps connect up to four separate normal faults (Figure 11a). The basalt conformably overlies horizontally stratified volcaniclastics and is truncated by the main Erkilet fault strand. There is no indication that the basalt flow cascaded down an already developing fault scarp; therefore, we interpret it to record onset of Erkilet fault activity. Fault slip indicators (Figure 13c) point to mostly N-S and NW-SE directed extension, oblique to the trace of the fault plane, but no significant left-lateral offset is observed in the faulted volcanics.

North of Kayseri, horst-and-graben structures (Figure 11b) are well exposed in the basin center. The Valibaba Tepe Ignimbrite and underlying pyroclastics record syndepositional faulting and are vertically displaced up to 10 m. Steep normal faults bounding the central basin structure strike N40°E and W35°S in the west and east, respectively (Figure 11b). The geometry of the fault planes suggests that the structure opens to the south and pinches to the north. Strain markers on major and minor faults are almost pure dip slip and indicate NW-SE extension (Figure 13c).

Vertical displacements across the Erkilet and Gesi faults were measured with GPS profiles (Figure 10b). For the Gesi fault vertical offset is constrained to 220 m, as measured by the offset of the Valibaba Tepe Ignimbrite on both sides of the fault. The Erkilet fault records a minimum vertical offset of 310 m, as the downthrown basalt is exposed in the hanging wall of only the first few step faults and is buried in the hanging wall beneath the Quaternary basin fill. Coupled with geochronological constraints for initiation of major activity on each fault (Erkilet: maximum interval of 2.22 ± 0.25 to present; Gesi: maximum interval of 2.73 ± 0.08 Ma to 1.0 ± 0.3 Ma) we are able to estimate minimum vertical displacement rates of ~0.10–0.18 mm a^{-1} on each fault and horizontal extension rates of less than 0.1 mm a^{-1}. These rates are minimums based on the average fault dip observed in the northern Erciyes basin, 68 ± 7° (n = 45). Considering that these two faults account for only 0.06–0.17 mm a^{-1} of extension across the basin, and modern, GPS-derived rates range up to 2 mm a^{-1} [*Aktuğ et al.*, 2013], additional extension is likely accommodated by buried, antithetic, and/or listric fault geometries at depth. An alternative scenario is recent acceleration of fault slip rate within the Erciyes basin.

5. Discussion

5.1. Quaternary Activity of the CAFZ

Original interpretations of the CAFZ by *Koçyiğit and Beyhan* [1998] argued for the presence of a major intracontinental shear zone crossing the entire Anatolian plate, developed in the Pliocene-Quaternary to

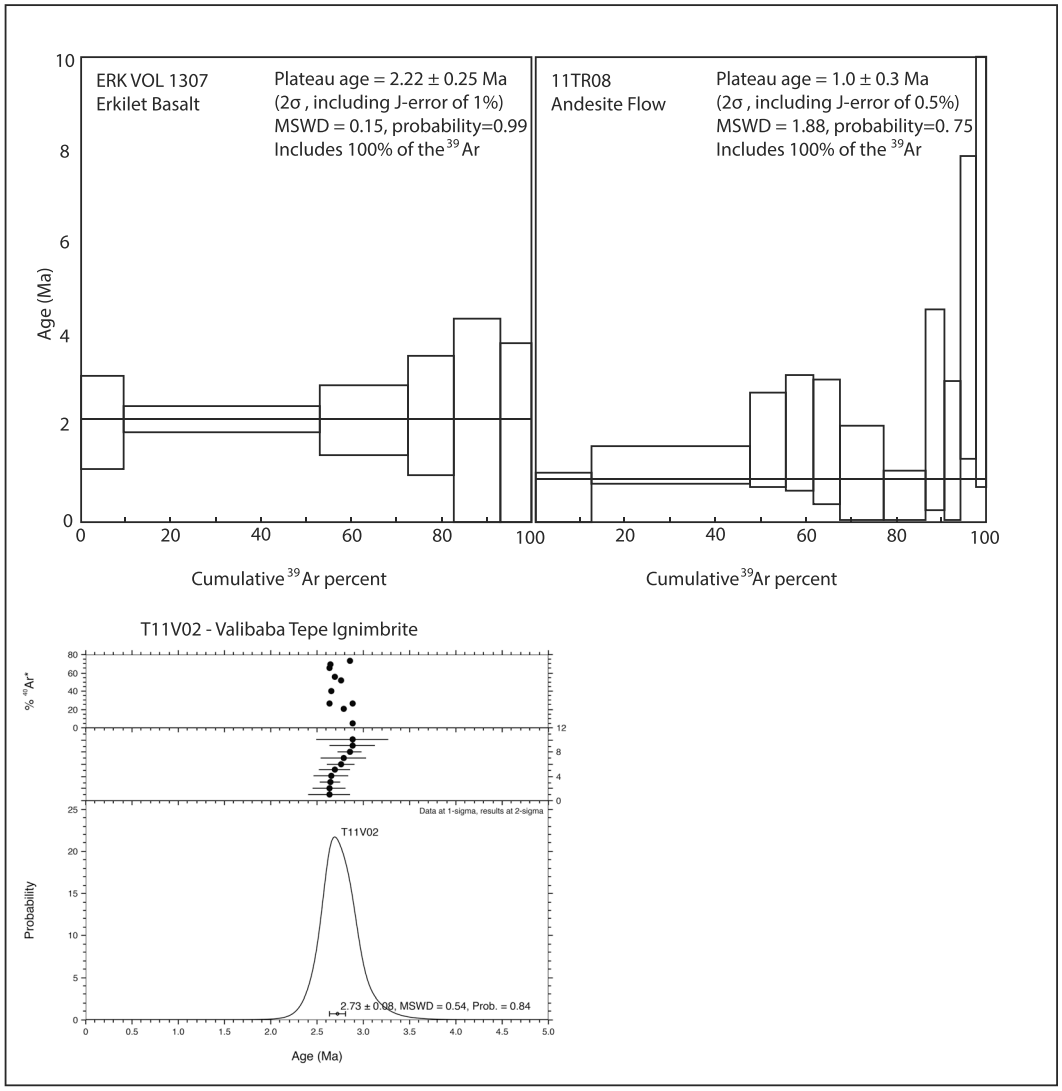

Figure 12. $^{40}Ar/^{39}Ar$ age (weighted plateau) derived from step heating of samples in the northern Erciyes basin. See Figure 10 for sample locations. T11V02 is an age probability diagram of single-crystal laser fusion of 10 individual plagioclase phenocrysts. The relatively large error associated with 11TR08 reflects the smaller analytical signal sizes associated with these potassium-poor grains.

accommodate the northward motion of the Arabian plate. Those authors proposed that the CAFZ developed a total neotectonic offset of up to 24 km and has an active slip rate of 3 mm a^{-1}. We question much of the evidence they proposed for the left-lateral nature and the continuity of the CAFZ.

The strongest evidence for an active component of sinistral displacement on the CAFZ comes from the Demirkazık-Sulucaova fault in the Ecemiş corridor. Displacement of the QAF-1 surface accumulated after the abandonment of the surface and before the formation of the QFT-1 surface, an interval of 52 ± 12 ka for the zero erosion case and 61 ± 14 ka for the 7 mm ka^{-1} erosion case. Combining this time interval with sinistral offsets ranging from 69 ± 5 m to 254 ± 3 m a range of minimum slip rates can be estimated. We agree with the interpretation of *Sarıkaya et al.* [2015b] that the ~250 m Fenk stream bend is a result of stream deflection around a rising topographic barrier and not a reliable marker of fault offset. However, we challenge their proposed piercing point that yield table 68 ± 2 m offset of the QAF-1 terrace riser north of the Yaluk stream (Figure 3b). No comparable offset of this feature was observed in the field or from satellite imagery. Additionally, terrace risers on the north side are displaced into the stream path and are therefore subject to reworking by erosion. We therefore consider the offset observed at the Marti River (Figure 5d) to be

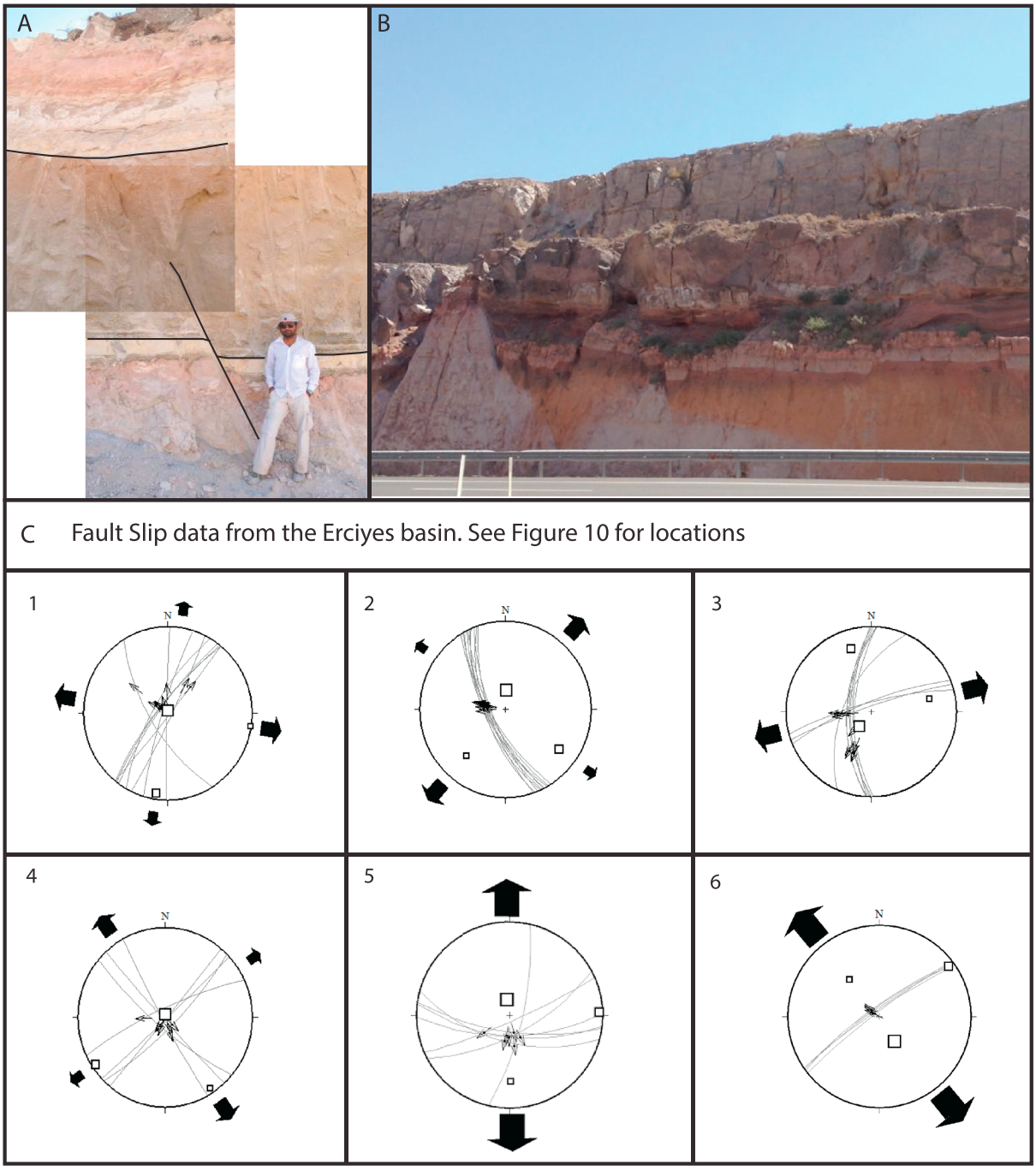

Figure 13. (a) Syndepositional faulting below the Valibaba Tepe Ignimbrite (2.73 ± 0.08 Ma) along the Gesi fault (left) and (b) central Erciyes basin. (c) Stereonets plotting fault planes and slip indicators from six sites in the northern Erciyes basin, see the map in Figure 10 for locations.

the most reliable. In this location, following displacement the terrace riser located downstream of the fault trace was sheltered from incision and has therefore evolved through diffusional processes to a gentler slope compared to the same riser located upstream of the fault. As a result the offset corner has been only slightly truncated by erosion. Our mapping suggests that left-lateral slip on datable geomorphic surfaces totals only 69 ± 5 m, which yields a minimum strike-slip rate of 1.1 ± 0.4 mm a^{-1} (erosion corrected) to 1.2 ± 0.4 mm a^{-1} (erosion and inheritance corrected) over the period. This is lower than the previous estimates (3 mm a^{-1} [*Koçyiğit and Beyhan*, 1998]). Using the maximum offset of 254 ± 3 m yields a minimum strike-slip rate

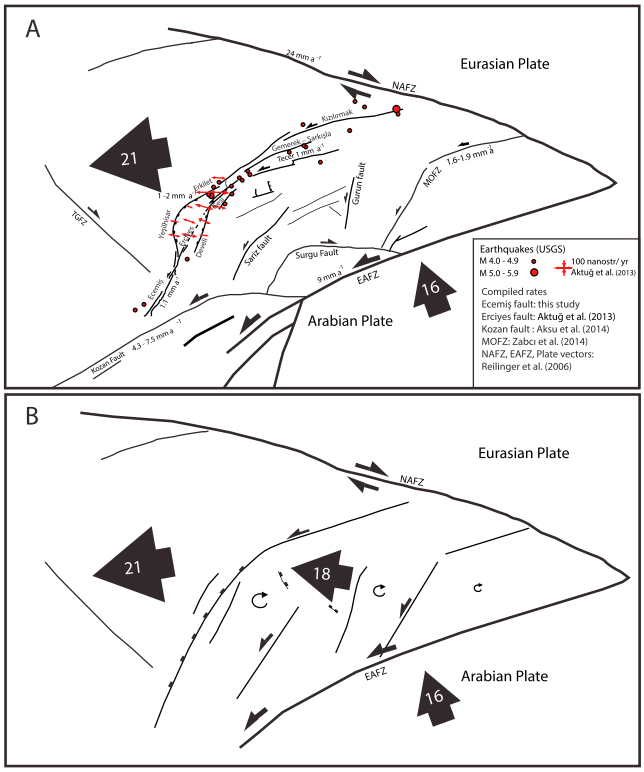

Figure 14. (a) Proposed model for Quaternary activity of the CAFZ, including regional deformation rates from this study and compiled from literature. Tecer fault [*Akyuz et al.*, 2013] and Malatya Ovacik fault zone (MOFZ) [*Zabci et al.*, 2014]. Plate vectors North Anatolian fault and East Anatolian fault from *Reilinger et al.* [2006]. Earthquakes from USGS earthquake catalogue [*Jenkins et al.*, 2013]. Strain indicators from *Aktuğ et al.* [2013]. (b) Proposed block model for the neotectonic framework of Central and Eastern Anatolia. The small circular arrows are small clockwise rotations which would accommodate a block model.

of 4.2 ± 1.2 mm a^{-1} (erosion corrected) to 4.4 ± 1.3 mm a^{-1} (erosion and inheritance corrected) over the period. For reasons mentioned above, we do not believe this offset amount and resulting slip rate to be accurate.

Although its slip rate remains difficult to constrain, the Demirkazık-Sulucaova fault has clearly not been active since abandonment of the QFT-1 surface at 44.5 ± 4.6 ka. In contrast, the west facing, range-front normal Cevizlık fault (Figure 3) records most of the recent activity in the Ecemiş corridor, with meter-scale scarps observed in young colluvium and a cumulative vertical offset of at least several hundred meters at the range front. These observations are consistent with *Aktuğ et al.*'s [2013] geodetic slip rates of less than slip 1 mm a^{-1} (sinistral) and 2 mm a^{-1} (extensional) [*Aktuğ et al.*, 2013]. We conclude that while the Ecemiş fault zone records left-lateral displacement during the late Quaternary, this is secondary to predominantly E-W extension, coeval with multiphase uplift of the Central Taurides (Figure 2) from 8 Ma to present [*Schildgen et al.*, 2012, 2014].

Evidence for a link between faults in the Ecemiş corridor and the Erciyes basin is tenuous. We interpret dacitic lava domes emplaced along the Dundarlı-Erciyes fault to record syneruptive extensional stress between 580 ± 130 and 210 ± 180 ka, with no sinistral component during that period or since dome emplacement. This finding refutes the attempt of *Jaffey et al.* [2004] to link late-Quaternary strike-slip activity between the Ecemiş and Dundarlı-Erciyes faults. Therefore, the most recent phase of late-Pleistocene strike-slip faulting described in the Ecemiş corridor is not kinematically linked to faulting farther north along the Erciyes fault. We also argue for an earlier onset of opening of the Erciyes basin than earlier studies [*Koçyiğit and Beyhan*, 1998; *Koçyiğit and Erol*, 2001; *Dirik*, 2001], which have speculated that it began after deposition of the youngest regionally extensive ignimbrite layer, the 2.73 ± 0.08 Ma Valibaba Tepe Ignimbrite, that is found on both margins of the basin. However, we observe that conformable pyroclastic rocks below the Valibaba Tepe Ignimbrite are syndepositionally deformed, suggesting earlier an earlier initiation of faulting. Ignimbrites are density currents that locally thicken in valleys and topographic lows but are capable of draping landscapes with minimal relief [*Branney and Kokelaar*, 2002] and therefore could have flowed up the margins of an already opening proto-Erciyes basin. Our study suggests dominantly extensional deformation in the northern Erciyes basin, with minimal evidence for sinistral displacement. Our measurements of faults in the northern Erciyes basin consistently display dominantly dip-slip kinematic indicators. This is consistent with a regional GPS strain analysis [*Aktuğ et al.*, 2013], which highlighted a zone of WNW-ESE extension in the Erciyes basin (Figure 14). We disagree with the use of polygenetic volcanoes along the border of the basin as piercing points [*Toprak*, 1998], which were used to estimate strike-slip offset and basin extension at 28 and 45 km, respectively (*X* to *Y* in Figure 2). Late Pliocene pyroclastics and the Valibaba Tepe Ignimbrite are preserved throughout the central basin, meaning that the width of the basin

is not a valid estimation of expansion or extension. Piercing points from the basin margins are therefore invalid as both a strike-slip and normal strain markers. Further, although *Koçyiğit and Beyhan* [1998] argue for dominantly left-lateral displacement along the Gesi fault, citing 2.2 km of left-lateral offset of the Yüzbaşı stream (Figure 10), we were unable to find any trace of a fault in the vicinity of this bend in the field, and we find no other gorges or smaller rivers which show similar offset. We attribute the bend instead to stochastic drainage variation.

We question the continuity and importance of the CAFZ beyond our study area as well. Faults in the far south-western part of the proposed CAFZ, including the Namrun fault and the offshore Cyprus-Anamur fault (Figure 1 [*Koçyiğit and Beyhan*, 1998]), make up over 300 km of the proposed 700 km fault zone. These strands are proposed to extend from the south of the Ecemiş corridor, connecting the fault zone to the Cyprus trench. Recent seismic reflection studies [*Aksu et al.*, 2014], however, show that these structures likely belong to the Kozan fault zone (Figure 2). The Kozan fault zone is a 300 km long, 15–20 km wide transtensional sinistral fault zone that splays from the triple junction between the East Anatolian fault and the Dead Sea fault zone and extends offshore near Adana, where it separates the Tauride Mountains to the north and the Cilicia and Adana basins to the south (Figure 2). *Aksu et al.* [2014] propose latest Messinian-Recent slip rates of 4.3–7.5 mm a^{-1} based on offset of sediment lobes imaged from seismic profiles. These rates are much higher than slip rates we have measured along the CAFZ. Their results, along with a high density of earthquakes, suggest that the Kozan fault zone is a more significant left-lateral structure and has accommodated partitioned strain that had previously been attributed to the CAFZ.

The northeast part of the CAFZ, from Erkilet to the North Anatolian fault, appears more continuous and seismically active. A small cluster of eight *M* 4.0 to 5.1 earthquakes have been recorded in the northern part of the Erciyes basin since 1985 (USGS [*Jenkins et al.*, 2013]), roughly delimiting the trace of Erkilet fault (Figure 14a) and suggest that it is still active. All of these events were located at depths of less than 10 km. The focal mechanisms of these faults were not available. *Akyuz et al.* [2013] compiled data for 11 earthquakes between *M* 3.0 and *M* 5.0 since 1960 that occurred on the Deliler and Teer faults of the NE part of the CAFZ. Six of these events were recorded at depths of less than 5 km. In the southern Erciyes basin and the Ecemiş fault zone, active seismicity does not delimit the CAFZ further to the south, where only sporadic events have been recorded.

In summary, skepticism about the continuity, left-lateral nature, Quaternary offset, and activity along the CAFZ is justified [*Westaway*, 1999; *Westaway et al.*, 2002]. Our results document Quaternary faulting with spatial connectivity, (i.e., the strong linear trend shared by the Ecemiş-Erciyes and Gesi faults), but we find no direct evidence of coeval motion along the length of the CAFZ, and everywhere they are measured, we find that faults are slipping slowly and often have become dormant or inactive. Finally, we find total neotectonic offset to be much less than the 24 to 28 km estimates from previous studies [*Koçyiğit and Beyhan*, 1998; *Toprak*, 1998].

5.2. Evolution of the CAFZ

Koçyiğit and Beyhan [1998] originally proposed that slip along the CAFZ began in the Ecemiş corridor and propagated to the northeast and southwest, eventually linking into a throughgoing structure that accommodated significant strike-slip displacement across the entire Anatolian plate (Figure 2). We propose a new model for the evolution of the CAFZ, in which two paleotectonic structures, the Ecemiş corridor in the southwest and the Inner Tauride suture zone in the northeast, were reactivated independently. These structures were then bridged together by a zone of active extension to produce the modern CAFZ.

In our proposed scenario, the NE part of the CAFZ developed into a broad NE-SW trending, sinistral strike-slip fault zone, including the Kızılırmak, Gemerek-Şarkışla, Deliler, and Tecer faults (Figure 14). They developed along preexisting weaknesses in the vicinity of the Inner Tauride suture zone as a result of compression in eastern Anatolia during the late Miocene to Quaternary [*Yılmaz and Yılmaz*, 2006; *Kaymakci et al.*, 2010]. Many of these faults remain seismically active, and slip rates of 1 mm a^{-1} have been proposed for the Tecer fault [*Akyuz et al.*, 2013]. Additional strain is likely distributed across this broad zone of faults. To the east, the Malatya-Ovacık fault zone (MOFZ; Figure14a) is of the same orientation and sense of shear [*Kaymakci et al.*, 2006; *Westaway et al.*, 2008; *Zabci et al.*, 2014]. Both of these structures may represent an array of en echelon antithetic faults accommodating strain along the North Anatolian fault. We suggest that internal deformation of the northeastern part of the Anatolian plate is predominantly strike slip and could be explained by a domino block faulting model with small amounts of clockwise rotation of crustal blocks

bounded by weakly active strike-slip faults (e.g., CAFZ, Malatya-Ovacık fault zone, and potentially the Sariz and Gürün faults) (Figure 14b). These small clockwise rotations between these blocks are consistent with an east to west transition from counterclockwise to clockwise rotations deduced from regional paleomagnetic data [*Piper et al.*, 2010].

Where the CAFZ bends to the south near the southern end of the Erkilet fault, it intersects a WNW-ESE extensional domain (Figure 14a) [*Aktuğ et al.*, 2013] and normal displacement along the fault increases. This extensional domain stretches from west of the Delier fault to the southern Erciyes basin (Figure 14). The resulting releasing bend observed along the Erkilet fault produced a horsetail splay and step-like morphologic patterns, which bend south and transition to pure normal faulting on the Yeşilhisar fault. Their kinematics is mirrored by the conjugate Develi fault in the SE margin of the basin, where the fault scarp has relief of $>$900 m [*Koçyiğit and Erol*, 2001]. WNW-ESE opening of the basin was coeval with growth of the Erciyes stratovolcano, and the same stress regime controlled emplacement of monogenetic dome alignment on its SW flank along the Erciyes fault. We propose that Erciyes fault cuts through the middle of the basin and aligns with the Ecemiş fault; extensional faulting is consistent with mountain front normal faulting in the Ecemiş corridor, where large vertical offset is observed at the mountain front near the Cevizlik fault. Normal faulting is accompanied by transtensional strike slip along the Demirkazık-Sulucaova fault. This WNW-ESE extensional stress field is likely related to the westward extrusion of Anatolia, primarily driven by the Western Anatolian extensional province. Given their orientation (NE to ENE) and the overall westward pull of Anatolia, small amounts of sinistral motion and larger amounts of horizontal extension are expected along these structures. Ongoing counterclockwise rotation of Central Anatolia toward the Hellenic trench has oriented this part of the CAFZ closer to N-S orientation. We propose that extensional faulting in the central and southern parts of the CAFZ accommodates the increasing E-W velocity gradient across the region (Figure 14b). A Pliocene-Quaternary changeover to NE-SW extensional along the Tuz Gölü fault zone has been attributed to the influence of the Western Anatolian extensional province [*Özsayin et al.*, 2013], and the results of this study support the suggestion that further extend this extensional influence as far east as the CAFZ [*Aktuğ et al.*, 2013].

With low slip rate and little evidence for major strike-slip offset during the Quaternary, the modern CAFZ cannot be characterized as a tectonic escape structure, such as the North Anatolian fault or East Anatolian fault. We prefer to characterize the modern CAFZ as a weakly active fault with nonuniform slip rates and spatially and kinematically linked zones of heterogeneous deformation in Central Anatolia. Second-order strike-slip fault systems within the Anatolian plate, such as the CAFZ and the Malatya-Ovacık fault zone, are likely shallow upper crustal structures that divide east and central Anatolia into smaller tectonic blocks that move relative to one another while also moving west with respect to Eurasia (Figure 14b). This interpretation is based on the shallow seismicity along the CAFZ and supported by low slip rates presented in this study as well the similarly low rates inferred along the Tecer fault (~1 mm/yr [*Akyuz et al.*, 2013]) and the Malatya-Ovacık fault zone (1.6–1.9 mm a^{-1} [*Zabci et al.*, 2014]). The variability in recent kinematics observed along the central part of the CAFZ (~350 km) can be explained by its propagation through rapidly transitioning N-S and E-W stress patterns (stress permutations), which are well defined within the Anatolian plate [*Aktuğ et al.*, 2013].

6. Conclusions

We have created new Quaternary fault maps and constrained kinematics and slip rates on important faults in the southern and central parts of the CAFZ. When compiled with additional neotectonic data (GPS, seismicity, and paleoseismology) the main conclusions of this study are as follows. Geomorphically derived slip rates on the Ecemiş fault zone of 1.1 ± 0.4 mm a^{-1} (erosion corrected) or 1.2 ± 0.4 mm a^{-1} (erosion and inheritance corrected) are lower than original estimates. These are comparable with other slip rate estimates of weakly active internal strike-slip faults of the Anatolian plate (Malatya-Ovacık fault zone 1.6–1.9 mm a^{-1} [*Zabci et al.*, 2014] and Teçer fault 1 mm a^{-1} [*Akyuz et al.*, 2013]) and are more an order of magnitude smaller than major plate bounding strike-slip faults (North Anatolian fault and East Anatolian fault). The most recent episodes of faulting in the Ecemiş corridor are not kinematically linked with faulting in the Erciyes basin. Most of the faulting in the Erciyes basin occurred between 2.73 ± 0.08 Ma (T11V02; Figure 12c) and 1.0 ± 0.3 Ma (11TR-08; Figure 12b), dominated by horizontal extension in a WNW-ESE direction. The combined effects of a strike-slip-releasing bend and extrusion-related crustal extension produced the modern basin topography. Previous attempts to estimate total left-lateral offset along the CAFZ from restoration of an

Erciyes "pull-apart" basin [*Koçyiğit and Beyhan*, 1998; *Toprak*, 1998; *Koçyiğit and Erol*, 2001] are much too large. Our alternative model for opening of the Erciyes basin by predominantly WNW-ESE extension is supported by kinematic, geomorphological, and geodetic data and suggests that the influence of the Western Anatolian extensional province on deformation patterns in Central Anatolia is greater than previously thought. Any strain partitioned from the Eastern Anatolian compressional province is mostly restricted to the NE part of the CAFZ.

Acknowledgments
This research was funded by NSF grant EAR-1109762, "Continental Dynamics: Central Anatolian Tectonics" to Jane Willenbring (University of Pennsylvania) and an NSERC Discovery grant to Schoenbohm (University of Toronto). The authors are grateful to Mustafa Bozkurt for logistical and field assistance. Editon Nathan Niemi (University of Michigan) and anonymous reviewer provided excellent feedback that significantly improved the manuscript. Any use of trade, product, or firm names is for descriptive purposes only and does not imply endorsement by the U.S. Government. $^{40}Ar/^{39}Ar$ data tables and expanded methodology can be found in the supporting information or by contacting the corresponding author (mark.higgins@mail.utoronto.ca). Satellite imagery is copyright DigitalGlobe, Inc. and provided through the Polar Geospatial Center (University of Minnesota - Twin Cities).

References

Aksu, A. E., S. Walsh-Kennedy, J. Hall, R. N. Hiscott, C. Yaltırak, S. D. Akhun, and G. Çifçi (2014), The Pliocene–Quaternary tectonic evolution of the Cilicia and Adana basins, eastern Mediterranean: Special reference to the development of the Kozan fault zone, *Tectonophysics*, *622*, 22–43.

Aktuğ, B., E. Parmaksız, M. Kurt, O. Lenk, A. Kılıçoğlu, M. A. Gürdal, and S. Özdemir (2013), Deformation of Central Anatolia: GPS implications, *J. Geodyn.*, *67*, 78–96.

Akyuz, H. S., G. Ucarkus, E. Altunel, B. Dogan, and A. Dikbas (2013), Paleoseismological investigations on a slow-moving active fault in Central Anatolia, Tecer Fault, Sivas, *Ann. Geophys.*, *55*(5), doi:10.4401/ag-5444.

Allen, M. B. (2010), Roles of strike-slip faults during continental deformation: Examples from the active Arabia–Eurasia collision, *Geol. Soc., London Spec. Publ.*, *338*(1), 329–344.

Barka, A., H. S. Akyüz, H. A. Cohen, and F. Watchorn (2000), Tectonic evolution of the Niksar and Tasova–Erbaa pull-apart basins, North Anatolian fault zone: Their significance for the motion of the Anatolian block, *Tectonophysics*, *322*(3), 243–264.

Biryol, C., S. L. Beck, G. Zandt, and A. A. Özacar (2011), Segmented African lithosphere beneath the Anatolian region inferred from teleseismic *P*-wave tomography, *Geophys. J. Int.*, *184*(3), 1037–1057.

Bozkurt, E. (2001), Neotectonics of Turkey—A synthesis, *Geod. Acta*, *14*(1), 3–30.

Branney, M. J., and B. P. Kokelaar (2002), Pyroclastic Density Currents and the Sedimentation of Ignimbrites, *Mem. Geol. Soc. London*, *27*.

Burke, K., and C. Sengör (1986), Tectonic escape in the evolution of the continental crust, *Geodyn. Ser.*, *14*, 41–53.

Cebriá, J. M., C. Martín-Escorza, J. López-Ruiz, D. J. Morán-Zenteno, and B. M. Martiny (2011), Numerical recognition of alignments in monogenetic volcanic areas: Examples from the Michoacán-Guanajuato volcanic field in Mexico and Calatrava in Spain, *J. Volcanol. Geotherm. Res.*, *201*(1), 73–82.

Çemen, İ., M. C. Göncüoglu, and K. Dirik (1999), Structural evolution of the Tuzgölü basin in Central Anatolia, Turkey, *J. Geol.*, *107*(6), 693–706.

Çetin, H. (2000, June), Paleoseismology of the Ecemiş fault: Mid results, in Workshop on Active Tectonics of Western Turkey, in Memoriam to Paul L. Hancock, İstanbul Tech. Univ., pp. 47–55.

Corazzato, C., and A. Tibaldi (2006), Fracture control on type, morphology and distribution of parasitic volcanic cones: An example from Mt. Etna, Italy, *J. Volcanol. Geotherm. Res.*, *158*(1), 177–194.

Cowgill, E. (2007), Impact of riser reconstructions on estimation of secular variation in rates of strike–slip faulting: Revisiting the Cherchen River site along the Altyn Tagh Fault, NW China, *Earth Planet. Sci. Lett.*, *254*(3), 239–255.

Desilets, D., and M. Zreda (2003), Spatial and temporal distribution of secondary cosmic-ray nucleon intensities and applications to in situ cosmogenic dating, *Earth Planet. Sci. Lett.*, *206*(1), 21–42.

Dewey, J. F., M. R. Hempton, W. S. F. Kidd, F. T. Saroglu, and A. M. C. Şengör (1986), Shortening of continental lithosphere: The neotectonics of Eastern Anatolia—A young collision zone, *Geol. Soc. London Spec. Publ.*, *19*(1), 1–36.

Dirik, K. (2001), Neotectonic evolution of the northwestward arched segment of the Central Anatolian fault zone, Central Anatolia, Turkey, *Geodyn. Acta*, *14*(1), 147–158.

Ercan, T., S. Tokel, J. I. Matsuda, T. Ui, K. Notsu, and T. Fujitani (1994), Erciyes dagi (Orta Anadolu) pliyo-kuvaterner volkanizmasina iliskin yeni jeokimyasal, izotopik, radyometrik veriler ve jeotermal enerji açısından onemi, *Turkiye*, *6*, 17–22.

Faccenna, C., O. Bellier, J. Martinod, C. Piromallo, and V. Regard (2006), Slab detachment beneath eastern Anatolia: A possible cause for the formation of the North Anatolian fault, *Earth Planet. Sci. Lett.*, *242*(1), 85–97.

Gans, C. R., S. L. Beck, G. Zandt, C. B. Biryol, and A. A. Ozacar (2009), Detecting the limit of slab break-off in central Turkey: New high-resolution Pn tomography results, *Geophys. J. Int.*, *179*(3), 1566–1572.

Gosse, J. C. (2011), Terrestrial Cosmogenic Nuclide Techniques for Assessing Exposure History of Surfaces and Sediments in Active Tectonic Regions, in *Tectonics of Sedimentary Basins: Recent Advances*, edited by C. Busby and A. Azor, John Wiley, Chichester, U. K., doi:10.1002/9781444347166.ch3.

Gosse, J. C., and F. M. Phillips (2001), Terrestrial in situ cosmogenic nuclides: Theory and application, *Quat. Sci. Rev.*, *20*(14), 1475–1560.

Heidbach, O., M. Tingay, A. Barth, J. Reinecker, D. Kurfeß, and B. Müller (2001), World stress map, *Naturwissenschaften*, *88*, 357–371.

Idleman, L., M. A. Cosca, M. T. Heizler, S. N. Thomson, C. Teyssier, and D. L. Whitney (2014), Tectonic burial and exhumation cycles tracked by muscovite and K-feldspar $^{40}Ar/^{39}Ar$ thermochronology in a strike-slip fault zone, central Turkey, *Tectonophysics*, *612*, 134–146.

Jaffey, N., and A. H. Robertson (2001), New sedimentological and structural data from the Ecemiş fault zone, southern Turkey: Implications for its timing and offset and the Cenozoic tectonic escape of Anatolia, *J. Geol. Soc.*, *158*(2), 367–378.

Jaffey, N., and A. Robertson (2005), Non-marine sedimentation associated with Oligocene-Recent exhumation and uplift of the Central Taurus Mountains, S Turkey, *Sediment. Geol.*, *173*(1), 53–89.

Jaffey, N., A. Robertson, and M. Pringle (2004), Latest Miocene and Pleistocene ages of faulting, determined by $^{40}Ar/^{39}Ar$ single-crystal dating of airfall tuff and silicic extrusives of the Erciyes Basin, central Turkey: Evidence for intraplate deformation related to the tectonic escape of Anatolia, *Terra Nova*, *16*(2), 45–53.

Jenkins, J., et al. (2013), Seismicity of the Earth 1900–2010 Middle East and vicinity, (ver. 1.1, Jan. 28, 2014), *U.S. Geol. Surv. Open File Rep., 2010–1083–K,* scale 1:7,000,000. [Available at http://pubs.usgs.gov/of/2010/1083/k/.]

Jolivet, L., and C. Faccenna (2000), Mediterranean extension and the Africa-Eurasia collision, *Tectonics*, *19*(6), 1095–1106, doi:10.1029/2000TC900018.

Kaymakci, N., M. Inceöz, and P. Ertepinar (2006), 3D-architecture and Neogene evolution of the Malatya Basin: Inferences for the kinematics of the Malatya and Ovacık fault zones, *Turk. J. Earth Sci.*, *15*(2), 123–154.

Kaymakci, N., M. Inceöz, P. Ertepinar, and A. Koç (2010), Late Cretaceous to recent kinematics of SE Anatolia (Turkey), *Geol. Soc. London Spec. Publ.*, *340*(1), 409–435.

Keskin, M. (2003), Magma generation by slab steepening and breakoff beneath a subduction-accretion complex: An alternative model for collision-related volcanism in Eastern Anatolia, Turkey, *Geophys. Res. Lett.*, *30*(24), 8046, doi:10.1029/2003GL018019.
Koç, A., and N. Kaymakcı (2013), Kinematics of Sürgü fault zone (Malatya, Turkey): A remote sensing study, *J. Geodyn.*, *65*, 292–307.
Koçyiğit, A., and A. Beyhan (1998), A new intracontinental transcurrent structure: The Central Anatolian fault zone, Turkey, *Tectonophysics*, *284*(3), 317–336.
Koçyiğit, A., and A. Beyhan (1999), Reply to Rob Westaway's comment on "A new intracontinental transcurrent structure: The Central Anatolian fault zone, Turkey", *Tectonophysics*, *314*(4), 481–496.
Koçyiğit, A., and O. Erol (2001), A tectonic escape structure: Erciyes pull-apart basin, Kayseri, central Anatolia, Turkey, *Geodin. Acta*, *14*(1), 133–145.
Koppers, A. A. P. (2002), ArArCALC—Software for $^{40}Ar/^{39}Ar$ age calculations, *C. R. Geosci.*, *28*(2002), 605–619.
Lacombe, O., F. Mouthereau, J. Angelier, and B. Deffontaines (2001), Structural, geodetic and seismological evidence for tectonic escape in SW Taiwan, *Tectonophysics*, *333*(1), 323–345.
Le Corvec, N., K. B. Spörli, J. Rowland, and J. Lindsay (2013), Spatial distribution and alignments of volcanic centers: Clues to the formation of monogenetic volcanic fields, *Earth Sci. Rev.*, *124*, 96–114.
Lifton, N., T. Sato, and T. J. Dunai (2014), Scaling "in situ" cosmogenic nuclide production rates using analytical approximations to atmospheric cosmic-ray fluxes, *Earth Planet. Sci. Lett.*, *386*, 149–160.
Ludwig, K. R. (2003), Isoplot 3.09: A geochronological toolkit for Microsoft Excel, Berkeley Geochronology Center, Spec. Publ., 4.
Marrero, S. (2012), Calibration of cosmogenic chlorine-36, Doctoral dissertation, New Mexico Inst. of Min. and Technol.
McClusky, S., S. Balassanian, A. Barka, C. Demir, S. Ergintav, I. Georgiev, and G. Veis (2000), Global Positioning System constraints on plate kinematics and dynamics in the eastern Mediterranean and Caucasus, *J. Geophys. Res.*, *105*(B3), 5695–5719, doi:10.1029/1999JB900351.
McKenzie, D. (1972), Active tectonics of the Mediterranean region, *Geophys. J. Int.*, *30*(2), 109–185.
McQuarrie, N., and D. J. van Hinsbergen (2013), Retrodeforming the Arabia-Eurasia collision zone: Age of collision versus magnitude of continental subduction, *Geology*, *41*(3), 315–318.
Mineral Research and Exploration General Directorate (MTA) (2002), Geological map of Turkey, Andana and Kayseri sheets, 1/500000 scale (2002 ed.) MTA, Anakara.
Nakamura, K. (1977), Volcanoes as possible indicators of tectonic stress orientation—Principle and proposal, *J. Volcanol. Geotherm. Res.*, *2*(1), 1–16.
Özsayin, E., T. A. Ciner, F. B. Rojay, R. K. Dirik, D. Melnick, and D. Fernandez-Blanco (2013), Plio-Quaternary extensional tectonics of the Central Anatolian Plateau: A case study from the Tuz Gölü Basin, Turkey, *Turk. J. Earth Sci.*, *22*(5), 691–714.
Paulsen, T. S., and T. J. Wilson (2010), New criteria for systematic mapping and reliability assessment of monogenetic volcanic vent alignments and elongate volcanic vents for crustal stress analyses, *Tectonophysics*, *482*(1), 16–28.
Piper, J. D. A., H. Gürsoy, O. Tatar, M. E. Beck, A. Rao, F. Koçbulut, and B. L. Mesci (2010), Distributed neotectonic deformation in the Anatolides of Turkey: A palaeomagnetic analysis, *Tectonophysics*, *488*(1), 31–50.
Redfield, T. F., D. W. Scholl, P. G. Fitzgerald, and M. E. Beck (2007), Escape tectonics and the extrusion of Alaska: Past, present, and future, *Geology*, *35*(11), 1039–1042.
Reilinger, R., et al. (2006), GPS constraints on continental deformation in the Africa-Arabia-Eurasia continental collision zone and implications for the dynamics of plate interactions, *J. Geophys. Res.*, *111*, B05411, doi:10.1029/2005JB004051.
Royer, D. L. (1999), Depth to pedogenic carbonate horizon as a paleoprecipitation indicator?, *Geology*, *27*(12), 1123–1126.
Rubin, A. M. (1995), Propagation of magma-filled cracks, *Annu. Rev. Earth Planet. Sci.*, *23*, 287–336.
Sarıkaya, M. A., C. Yıldırım, and A. Çiner (2015a), Late Quaternary alluvial fans of Emli Valley in the Ecemiş fault zone, south central Turkey: Insights from cosmogenic nuclides, *Geomorphology*, *228*, 512–525.
Sarıkaya, M. A., C. Yıldırım, and A. Çiner (2015b), No surface breaking on the Ecemis Fault, central Turkey, since Late Pleistocene (~64.5 ka); new geomorphic and geochronologic data from cosmogenic dating of offset alluvial fans, *Tectonophysics*, *649*, 33–46.
Schildgen, T. F., D. Cosentino, B. Bookhagen, S. Niedermann, C. Yıldırım, H. Echtler, H. Wittmann, and M. R. Strecker (2012), Multi-phased uplift of the southern margin of the Central Anatolian Plateau, Turkey: A record of tectonic and upper mantle processes, *Earth Planet. Sci. Lett.*, *317*, 85–95.
Schildgen, T. F., C. Yıldırım, D. Cosentino, and M. R. Strecker (2014), Linking slab break-off, Hellenic trench retreat, and uplift of the Central and Eastern Anatolian plateaus, *Earth Sci. Rev.*, *128*, 147–168.
Şen, E., B. Kürkcüoğlu, E. Aydar, A. Gourgaud, and P. M. Vincent (2003), Volcanological evolution of Mount Erciyes stratovolcano and origin of the Valibaba Tepe ignimbrite (Central Anatolia, Turkey), *J. Volcanol. Geotherm. Res.*, *125*(3), 225–246.
Şengör, A. M., and Y. Yılmaz (1981), Tethyan evolution of Turkey: A plate tectonic approach, *Tectonophysics*, *75*(3), 181–241.
Şengör, A. M. C. (1985), *Strike-Slip Faulting and Related Basin Formation in Zones of Tectonic Escape: Turkey as a Case Study*.
Şengör, A. M. C., S. Özeren, T. Genç, and E. Zor (2003), East Anatolian high plateau as a mantle-supported, north-south shortened domal structure, *Geophys. Res. Lett.*, *30*(24), 8045, doi:10.1029/2003GL017858.
Şengör, A. M. C., O. Tüysüz, C. Imren, M. Sakinç, H. Eyidogan, N. Görür, X. Le Pichon, and C. Rangin (2005), The North Anatolian fault: A new look, *Annu. Rev. Earth Planet. Sci.*, *33*, 37–112.
Stokes, M., D. J. Nash, and A. M. Harvey (2007), Calcrete "fossilisation" of alluvial fans in SE Spain: The roles of groundwater, pedogenic processes and fan dynamics in calcrete development, *Geomorphology*, *85*(1), 63–84.
Stone, J. O., G. L. Allan, L. K. Fifield, and R. G. Cresswell (1996), Cosmogenic chlorine-36 from calcium spallation, *Geochim. Cosmochim. Acta*, *60*(4), 679–692.
Straub, C., H. G. Kahle, and C. Schindler (1997), GPS and geologic estimates of the tectonic activity in the Marmara Sea region, NW Anatolia, *J. Geophys. Res.*, *102*(B12), 27,587–27,601, doi:10.1029/97JB02563.
Tapponnier, P., G. Peltzer, A. Y. Le Dain, R. Armijo, and P. Cobbold (1982), Propagating extrusion tectonics in Asia: New insights from simple experiments with plasticine, *Geology*, *10*(12), 611–616.
Toprak, V. (1998), Vent distribution and its relation to regional tectonics, Cappadocian Volcanics, Turkey, *J. Volcanol. Geotherm. Res.*, *85*(1), 55–67.
Umhoefer, P. J., D. L. Whitney, C. Teyssier, A. K. Fayon, G. Casale, and M. T. Heizler (2007), Yo-yo tectonics in a wrench zone, Central Anatolian fault zone, Turkey, *Geol. Soc. Am. Spec. Pap.*, *434*, 35–57.
Westaway, R. (1999), Comment on "A new intracontinental transcurrent structure: The Central Anatolian fault zone, Turkey" by A. Koçyiğit and A. Beyhan, *Tectonophysics*, *314*(4), 469–479.
Westaway, R., and J. Arger (2001), Kinematics of the Malatya–Ovacık fault zone, *Geodin. Acta*, *14*(1), 103–131.
Westaway, R., N. Jaffey, and A. H. F. Robertson (2002), Discussion of new sedimentological and structural data from the Ecemiş fault zone, southern Turkey: Implications for its timing and offset and the Cenozoic tectonic escape of Anatolia, *J. Geol. Soc.*, *159*(1), 111–113.
Westaway, R., T. Demir, and A. Seyrek (2008), Geometry of the Turkey-Arabia and Africa-Arabia plate boundaries in the latest Miocene to mid-Pliocene: The role of the Malatya-Ovacık fault zone in eastern Turkey, *eEarth*, *3*(1), 27–35.

Yetiş, C. (1984), New observations on the age of the Ecemiş Fault, in *Proc. of International Symposium on the Geology of the Taurus Belt*, pp. 159–164, Ankara.

Yılmaz, A., and H. Yılmaz (2006), Characteristic features and structural evolution of a post collisional basin: The Sivas Basin, Central Anatolia, Turkey, *J. Asian Earth Sci.*, *27*(2), 164–176.

Yilmaz, H., S. Over, and S. Ozden (2006), Kinematics of the East Anatolian fault zone between Turkoğlu (Kahramanmaras) and Celikhan (Adiyaman), eastern Turkey, *Earth Planets Space*, *58*, 1463–1473.

Zabci, C., T. Sançar, D. Tikhomirov, C. Vockenhuber, S. Ivy-Ochs, and N. Akçar (2014, May), Preliminary geologic slip rates of the Ovacik segment (Malatya-Ovacik Fault, Turkey) for the last 15 ka: Insights from cosmogenic ^{36}Cl dating of offset fluvial surfaces, In EGU General Assembly Conference Abstracts, 16, p. 9761.

Zreda, M., A. Çiner, M. A. Sarıkaya, C. Zweck, and S. Bayarı (2011), Remarkably extensive glaciation and fast deglaciation and climate change in Turkey near the Pleistocene-Holocene boundary, *Geology*, *39*(11), 1051–1054.